Fast reconstruction of motion from multielectrode records of retinal ganglion cells

Von der Fakultät für Mathematik und Naturwissenschaften
der Carl von Ossietzky Universität Oldenburg
zur Erlangung des Grades und Titels eines Doktors der Naturwissenschaften
– Dr. rer. nat. –
angenommene Dissertation
von

Herrn Edwin Alexander Cerquera Soacha

geboren am 12. August 1978 in Bogota, Republik Kolumbien

Gutachter: Priv.-Doz. Dr. Jan A. Freund

Zweitgutachterin: Prof. Dr. Jutta Kretzberg

Tag der Disputation: 06.07.2010
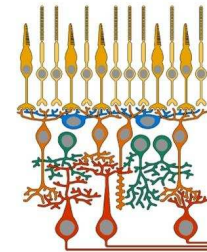
Zusammenfassung

Bewegung ist eine der Eigenschaften visueller Szenen, welche von der Retina kodiert werden müssen. Dieser Kode ist in den Aktionspotentialfolgen (Spike Trains) retinaler Ganglienzellpopulationen repräsentiert und wird über den optischen Nerv an das Gehirn übertragen. Die hohe Geschwindigkeit dieses Prozesses spiegelt die Herausforderung durch die Natur wider, welcher das visuelle System durch schnelle und effiziente Kodierung nachkommt. Die dieser Arbeit zugrunde liegenden Untersuchungen wurden anhand extrazellulärer Ganglienzell-Populationsantworten durchgeführt, die aus der isolierten Retina der Schildkröte *Pseudemys scripta elegans* gewonnen wurden. Die Retina wurde hierbei durch ein bewegtes Lichtmuster stimuliert. Ein Ziel der Arbeit war es zu prüfen, ob eine Subpopulation systematisch ausgewählter Zellen einer zufällig ausgewählten signifikant überlegen ist. Ausserdem wurden verschiedene schnelle Kodierungsstrategien unterschiedlicher Komplexität vergleichend bewertet. Alle diese Kodierungsstrategien bezogen nicht mehr als drei Aktionspotentiale pro Zelle ein, welche innerhalb eines Zeitfensters von 150 ms nach einer internen Referenz ausgelöst wurden. Diese frühen Spikes der gesamten Population wurden im Rahmen einer linearen Diskriminanzanalyse zur Rekonstruktion der Bewegungsreize verwandt. Die Resultate der Analysen weisen deutlich die Überlegenheit ausgewählter Subpopulationen nach. Darüber hinaus resultiert nur eine geringfügige Verbesserung aus der Hinzunahme weiterer Spikes im Anschluss an den jeweils ersten, welcher die Latenzkodierung definiert. Schliesslich erlaubt eine Kombination beider Teilergebnisse die Bestimmung einer optimalen Zellanzahl für die schnelle und effiziente Stimulusrekonstruktion.

Summary

Motion is one of the properties of visual scenes that must be encoded by the retina. This code is represented by spike trains produced by populations of retinal ganglion cells and transmitted via the optical nerve to the brain. This is a quick process that represents a natural challenge for the visual system to encode and decode visual information in a fast and efficient way. The analyses of this thesis were carried out on extracellular responses of a population of retinal ganglion cells from the isolated retina of a turtle *Pseudemys scripta elegans*. The retina was stimulated using a moving light pattern. One of the goals of this work was to check if selected cell sub-populations were significantly superior to randomly selected ones. Additionally, a set of fast coding strategies of different complexity were evaluated in a comparative manner. These coding strategies involved no more than the first three spikes per cell fired within a time window of 150 ms following an internal reference. These early spikes of the whole population were employed to reconstruct the stimuli using a classifier based on linear discriminant analysis. Our results indeed prove the superiority of selected sub-populations. Moreover, only a minor improvement results from including spikes following the first one defining the latency code. Finally, the combination of both results allows to determine an optimal number of cells for fast and efficient stimuli reconstruction.

List of publications

Manuscripts

Alexander Cerquera and Jan Freund. *Fast Estimation of Motion from Selected Populations of Retinal Ganglion Cells.* Submitted for Biological Cybernetics, March 2010.

Proceedings

Alexander Cerquera, Martin Greschner and Jan Freund. *Classifying the motion of visual stimuli from the spike response of a population of retinal ganglion cells.* 9th Proceedings of the 30th Annual International Conference of the IEEE Engineering in Medicine and Biology Society (EMBC) August 20-24. Vancouver, Canada, 2008. **Poster**

Alexander Cerquera, Martin Greschner and Jan Freund. *Classification of One-Dimensional Motion from Few Spikes of a Selected Retinal Ganglion Cell Population.* 9th Proceedings of the XII Symposium of Artificial Vision and Signals-Images Processing (STSIVA) September 10th-12th, 2008. Bucaramanga, Colombia. **Oral presentation**

Abstracts

Alexander Cerquera and Jan Freund. *Characterization of visual stimuli in retinal ganglion cells of the turtle by means of reliability analysis of multielectrode data.* 9th Inaugural Symposium of the Computational Vision & Neuroscience Group. April 7-8, 2008. Tübingen, Germany. **Poster**

Alexander Cerquera and Jan Freund. *Decoding of motions with multielectrode data acquired from a retinal ganglion cell population.* 9th 8th Göttingen Meeting of the German Neuroscience Society. March 25-29, 2009. Göttingen, Germany. **Poster**

Alexander Cerquera and Jan Freund. *Fast decoding and reconstruction of motions using multi-electrode information from retinal ganglion cells.* 9th European Retina Meeting. October 8-10, 2009. Oldenburg, Germany. **Poster**

Contents

Chapter 1

Introduction

1.1   The retina

The vertebrate retina is a neural network composed by several types of cells organized in form of layers and placed on the posterior inner surface of the eyeball. The retina tissue is constituted by: a) photoreceptors, b) horizontal cells, c) bipolar cells, d) amacrine cells and e) ganglion cells. The organization of these layers is presented in Figure 1.1. The main function of the retina is to encode the characteristics involved in any visual scene, i.e. color, contrast, surroundings, brightness, shapes, motions, etc. This code is produced finally by the layer of ganglion cells in form of electrical signals that are transmitted by the optic nerve to different areas of the brain for decoding and reconstruction of images (Dayan and Abbott, 2001, pp. 51-54). The retina originates during the embryonic stage, when the brain develops and some of its nerve fibers prolongate in outwards sense. Therefore, the retina is considered part of the central nerve system. The first stage of the early visual processing is the layer of photoreceptors, whose input is the visual information in form of light stimuli or photons that come from the environment passing through the entire eyeball. Before light reaches the photoreceptors it finds a dark epithelium, which prevents reflections into the layer of photoreceptors and protects the cells from excessive light radiation. A brief description about the cells that compose the retina and their functions for encoding of visual information are presented below.
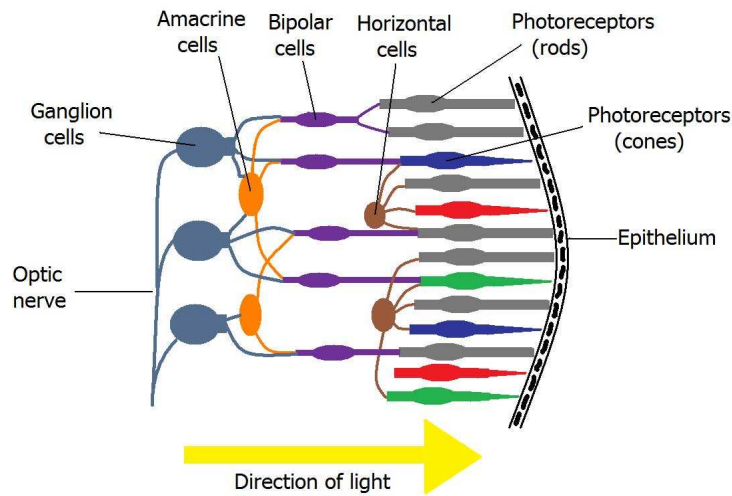
Figure 1.1: Simplified schematic distribution of the cellular layers in the retina. It can be noticed that light stimulus must go through all layers of the retina before reaching the photoreceptors.

1.1.1 Photoreceptors

As mentioned above, encoding of the visual information starts when light signals (photons) go through the anterior surface of the eye and reach the layer of retinal cells composed by photoreceptors (rods and cones), which transduce light stimuli into electrical signals. The number of rods and cones depends on species and whether their active life is predominantly diurnal or nocturnal. The function of rods is to capture the few photons available in environmental conditions with low light levels, whereas cones are responsible for encoding of colors present in visual scenes with adequate lighting (Wässle, 2004). Usually, the membranes of the photoreceptors are in contact with the epithelium and contain a protein known as opsin, which in turn bears a variation of vitamin A called retinal. This complex is called rhodopsin in rods and photopsin in cones. In this way, when photons fall into the layer of photoreceptors, are absorbed by these molecules and the signal transduction of light stimuli initiates. In normal darkness conditions, both cones and rods release to horizontal cells and bipolar cells an excitatory neurotransmitter known as glutamate.

1.1.2   Horizontal cells

Horizontal cells interconnect laterally groups of photoreceptors and dendrites of bipolar cells providing inhibitory signals that cause lateral inhibition. These inhibitory signals are produced when another neurotransmitter known as GABA (Gamma-Aminobutyric acid) is released by horizontal cells. In this way, when a photoreceptor is stimulated by light, the photoreceptor hyperpolarizes and glutamate release is reduced. In turn, GABA release from horizontal cells is also reduced causing an inhibitory effect on the photoreceptors and a negative feedback. The introduction of this lateral inhibition by horizontal cells avoids that the excitatory signal spreads around wide areas of the retina, limiting the action of the light stimulus inside the respective receptive field. This mechanism is important for detection of borders and contrast encoding.

1.1.3   Bipolar cells

Bipolar cells transmit signals from the photoreceptors layer to the ganglion cells layer. Their inputs are synaptically connected with the axons from either rods or cones, reason why they are denoted as rod bipolar or cone bipolar cells according to the type of photoreceptor connected to their inputs. Moreover, only one rods connect with their respective bipolar cell, whereas more than one cone may connect to a single bipolar cell. It is worth pointing out that cone bipolar cells connect directly to ganglion cells, whereas rod bipolar cells synapse initially to amacrine cells before transmitting signals to ganglion cells. These connections allow the transmission of signals from photoreceptors to amacrine and ganglion cells in separated and specialized channels. Both rod and cone bipolar cells are also classified into two types: ON and OFF. This classification depends on their reaction when glutamate is released by the photoreceptors. Normally, the photoreceptors are hyperpolarized when they detect photons and the release of glutamate decreases, so ON bipolar cells depolarize (or activate) and OFF bipolar cells hyperpolarize (or deactivate). Both ON and OFF bipolar cells tile the retina, providing an additional mechanism for detection of edge contrast even when the edge is located exactly between two adjacent photoreceptors.

1.1.4 Amacrine cells

There exists a wide variety of amacrine cells whose presence and functions depend on species (Kolb, 2003). These cells can be classified according to their morphological types, although the functions of most of them have not yet been totally understood. However, a special type of amacrine cell known as AII has been well studied. AII amacrine cells release glycine as neurotransmitter and their inputs are connected to ON rod bipolar cells, which means that an AII cell activates when center of its receptive field is stimulated by presence of light. In this way, AII cells collect information from rod bipolar cells and convey simultaneously via gap junctions depolarizing signals to ON (ON cone bipolar cell and ON ganglion cells) and OFF systems (OFF cone bipolar cell and OFF ganglion cells). AII cells associate in turn with another type of amacrine cells called A17 in order to convey signals to ganglion cells. These cells release GABA as neurotransmitter and collect also information from rod bipolar cells to amplify and modulate the signals that are transmitted from rod bipolar cells to AII cells. Nevertheless, it is not yet completely understood how A17 cells perform this function (Kolb, 2003). In general terms, there exists evidences that the role of amacrine cells involves enhancing vision in dim light environments, lateral inhibition between bipolar and ganglion cells and, possibly, a complementary definition of center and surround in receptive fields further than the performed by horizontal cells.

1.1.5 Ganglion cells

The layer of retinal ganglion cells (currently known with the acronym RGC) is the final stage of visual information processing in the retina. Ganglion cells receive signals from bipolar and amacrine cells establishing connexions with their ON and OFF pair systems, so they are classified in two types: ON and OFF. In this way, ON center ganglion cells activate when a spot of light stimulates the center of its receptive field if inactivates when the stimulation is produced on the surround. On the other hand, OFF center ganglion cells inactivate when light falls onto the central area of the receptive field and activates when light stimulates the perifery. This mechanism entails that the ganglion cells transmit information about contrast of a visual scene based on differences in firing

rates in the center and surround of the receptive field. Furthermore, processing of the spatial frequency in a visual scene depends on the size of the receptive field; high spatial frequencies stimulate small receptive fields, whereas low spatial frequencies stimulate large receptive fields. Figure 1.2 represents how ON and OFF ganglion cells response to light stimuli depending whether this falls either onto the center or the surround of their receptive fields.
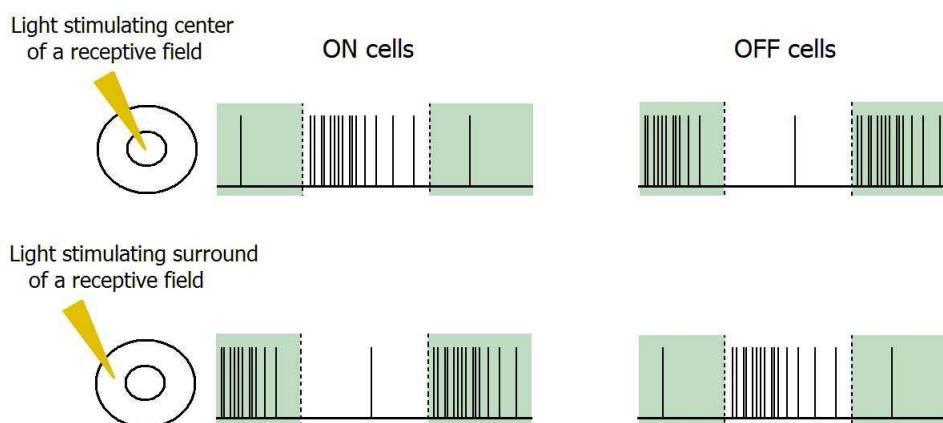
Figure 1.2: Responses of ON and OFF ganglion cells depending on the area of their receptive fields stimulated by spot lights.

Certain types of ganglion cells are tuned to detect different features of visual scenes, such as wavelength (color), size, brightness and motion. A special type of ganglion cells that detect sudden changes in visual scenes and react to spatiotemporal contrast modulations are Y cell, which produce transient responses and are considered as triggers of visual alerting functions (Demb and Sterling, 2001; Demb et al., 2001). Y cells are in turn classified in ON and OFF types; they are the largest ganglion cells in the retina and have the capacity to transmit information faster than other types of ganglion cells. Although only 5% of ganglion cells are Y cells, their dendrites are enough large to collect information from extensive retinal areas, in such a way that Y cells have wide receptive fields. Moreover, Y cells perform a nonlinear summation of their inputs. For this reason, they are sensitive to small and sudden motion detected in areas beyond their receptive fields, which is probably mediated by some amacrine cells (Demb et al., 1999).

There exist also specific direction selective ganglion cells, whose activity

was been initially modeled by Barlow and Levick (1965). According with this model, a direction selective (DS) ganglion cell receives information from two neighbouring image locations, by means of one excitatory input and one delayed inhibitory input (Figure 1.3a). The DS cell reacts to a motion in the preferred direction but not in the null direction. More recently, a model described by Fried et al. (2002, 2004) establishes interactions between excitatory and inhibitory inputs that differ between the preferred and the null direction (Figure 1.3b). The DS ganglion cells receive direct excitatory inputs from the preferred side and direct inhibitory inputs from the null side. The excitatory inputs in turn receive presynaptic inhibition from the null sides, whereas the inhibitory inputs receive presynaptic inhibition from the preferred sides.
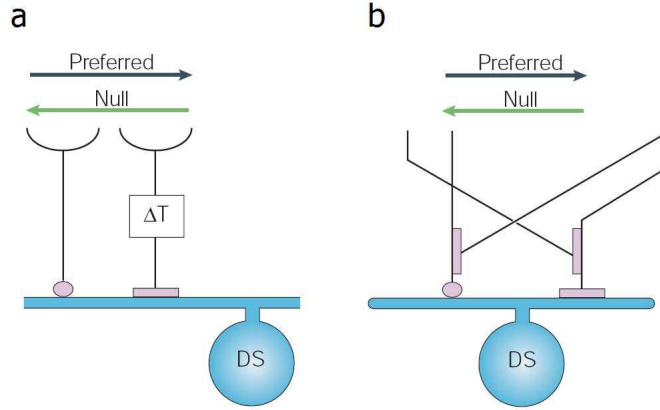
Figure 1.3: Scheme proposed to model the functions of direction-selective (DS) ganglion cells. a) initial model proposed by Barlow and Levick (1965). b) model presented by Fried et al. (2004). In both cases, the cells receive excitatory (left) and inhibitory (right) inputs (This figure has been taken modified from Wässle (2004)).

The output of the ganglion cells are temporal sequences of sharp depolarization electric waves, which are commonly denominated in the literature as action potentials or spikes. These signals are triggered inside the ganglion cells by voltage-gated ion channels in the cell membrane when the membrane potential reaches a high-enough level (Gollisch, 2009). Thus, the encoded visual information is contained in the temporal sequences of these spike trains (review: Meister and Berry, 1999). Subsequently, the signals are transmitted into

the brain via optic nerve for the corresponding decoding and reconstruction of the images or visual scenes.

1.2 Coding strategies

As mentioned in Section 1.1.5, the encoded visual information is contained in the spike trains fired by the ganglion cells layer and depend highly on the nature of the visual stimulus that is arriving into the retina; one or more spikes can be fired when a ganglion cell depolarizes in response to a stimulus. A prototype of one of these spikes is depicted in the upper panel of Figure 1.4. Normally, analysis of neural code is not focused on the shape of these spikes, but on the times in which their peaks (or eventually their valleys) are located, as well as the number of spikes (spike count) fired within a time window (Figure 1.4 lower panel). Basically, three coding strategies can be evaluated for analysis of retinal code: a) spike count, b) latency and c) spike timing, which are described in the following Subsections.
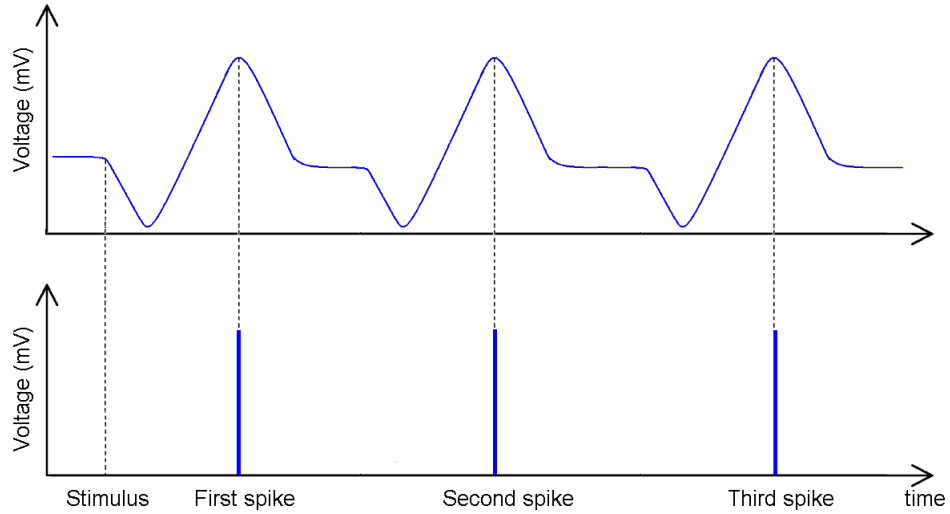
Figure 1.4: Representation of three spikes fired by a neuron after its stimulation.

1.2.1 Spike count

A first attempt for analysis of neural code based on spike count was presented by Adrian (1926). This approach established that the number of spikes produced by a neuron depends on how strong is the stimulus, i.e. the stronger the stimulus, the higher frequency of fired spikes by a neuron (or a population of neurons). Spike count may be evaluated estimating the number of spikes elicited in a time window over several trials of a stimulus, whose averaging leads to the construction of a post-stimulus time histogram (PSTH) such as described in Figure 1.5.
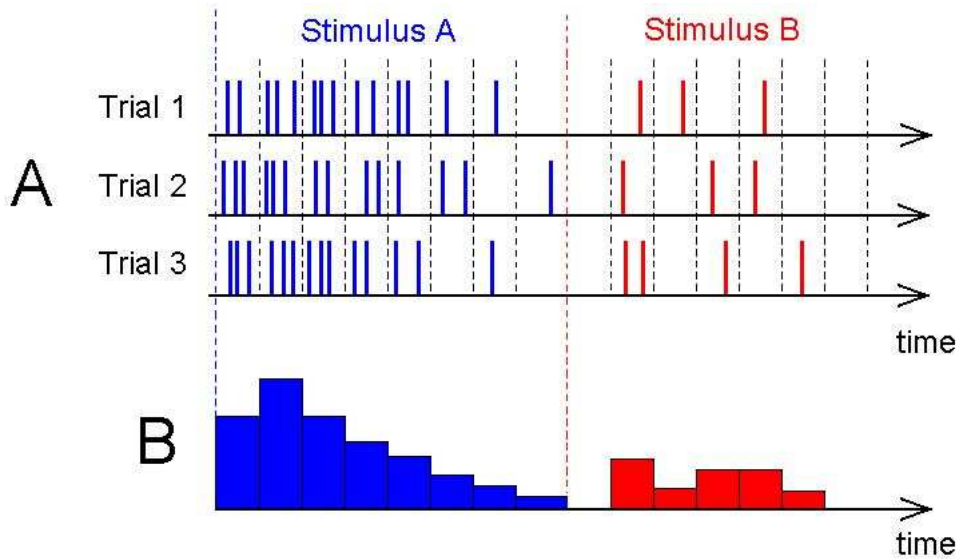
Figure 1.5: Scheme of the spikes elicited by a neuron in three trials. A. The number of spikes in each time window depends on the stimulus. B. Post-stimulus time histogram (PSTH) calculated when the number of spikes elicited in each bin across trials is averaged.

As can be noticed, a reliable and efficient evaluation of spike count demands long observation periods and many redundant neurons. This situation is incompatible with the sensory processing due to the extremely short integration time of the nervous system and the reaction speed of the brain. On the other hand, neurons in vertebrate retina fire with remarkable precision (Meister and Berry, 1999; Uzzell and Chichilnisky, 2004), for which spike timing information may be ignored in retinal codes based on spike count. For these reasons,

reconstruction of visual stimuli by evaluation and decoding of spike count is not biologically realistic (Gautrais and Thorpe, 1998).

1.2.2 Latency

Transmission of information from photoreceptors to ganglion cells requires a time that normally depends on the properties of the stimulus. Generally, this time is inversely proportional to spike count, i.e. strong stimuli induce high spike counts and short latencies, whereas weak stimuli provoke the opposite situation [1]. For this reason, the first spike that conveys the encoded visual information is fired with a delay from the temporal onset of the arriving stimulus. This time is known as latency, which could be sufficient for encoding purposes from a ideal point of view (Gerstner and Kistler, 2002, pp. 20-21). In contrast to spike count, a code based on latency turns out quite fast and efficient to evaluate. Theoretically, no spike is fired always in the same time point when a neuron responds to a repeated stimulus, but this time point variates within a time window (Figure 1.6A). The cause of this fact is the component of stochasticity found in the spike trains from single neurons or populations of neurons. Therefore, the encoded information provided by latency can be analyzed from the probability distribution obtained from the variations of these time points (Figure 1.6B).

Two kinds of latency can be defined: external latency and relative latency. External latency refers to the standard definition of latency that has been mentioned in the last paragraph, i.e. the time between the onset of the stimulus and the time point in which the first spike is fired. In biological sense, this approach is feasible only if the brain obtains information about the exact time of the onset. One probably biological source of this reference could be supplied when information about an oncoming movement is produced as a corollary discharge of the neuronal movement commands (Sommer and Wurtz, 2002), even though decoding by evaluation of external latency may not be feasible if the change of stimulus is produced externally. Instead, a code based on relative latency can be analyzed without prior knowledgment of any external onset. In

---

[1]This assumption is not always true; one exception of this rule are the biphasic OFF ganglion cells in the salamander retina (see (Gollisch and Meister, 2008)).
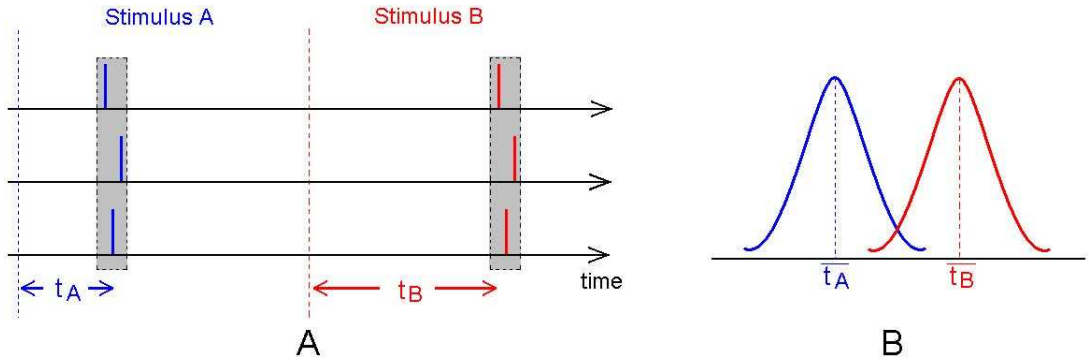
Figure 1.6: Representation of the latency times of a neuron according to two different stimuli. A. A strong stimulus (stimulus A) provokes responses with short latencies, whereas a weak stimulus (stimulus B) provokes the opposite situation. B. Scheme of the distribution probabilities for the two latency responses denoted as t_A and t_B respectively.

this approach, the relative onset may be estimated averaging the activity of a population of neurons. In this sense, Gollisch (2009) argues that this information in relative spike timing could be detected by downstream brain regions through delay lines and coincidence detection (Figure 1.6B). The explanation of this behavior is the strong correlation of the times in which the first spikes are fired among a population of ganglion cells; one cell tends to fire a spike following another one that fired a spike some milliseconds ago. This mechanism could be caused by the electrical connections among nearby ganglion cells through gap junctions, which induce concerted firing patterns whose latencies can be narrowly synchronized in times less than 3 ms (Brivanlou et al., 1998; Hu and Bloomfield, 2003). Another correlated neuronal activity can be found due to shared input into ganglion cells from bipolar or amacrine cells (Levine, 1997; Murphy and Rieke, 2008).

1.2.3 Spike timing

Spike timing refers basically to the analysis of the time points in which a neuron (or a population of neurons) fires its spikes in response to a stimulus (review: Lestienne, 2001), so it may be suggested that this coding strategy
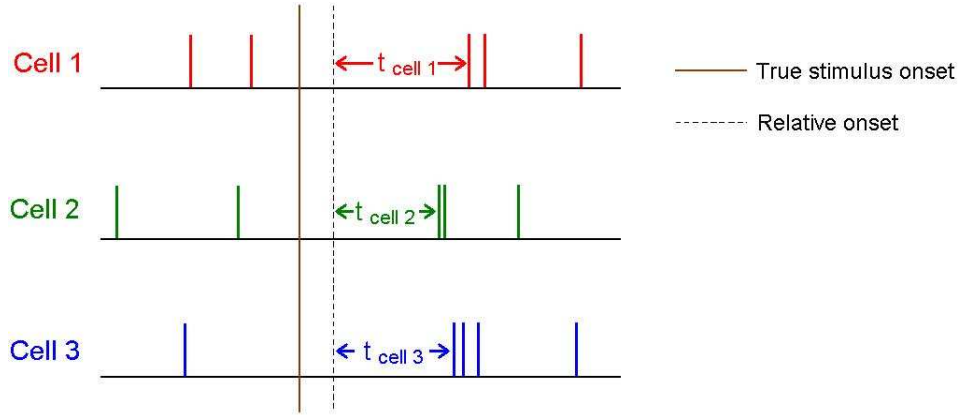
Figure 1.7: Scheme of relative latency from a population of three cells denoted as cell A, cell B and cell C. The temporal information of the first spike (latency) fired by each cell is referred to the time in which changes in the average of the population activity occur (dotted line).

may convey more detailed information than spike count and latency. Moreover, spike timing can be thought as an extension of the latency, because it is not only analyzed the temporal information of the first spike, but of all the spikes fired within a time window. Such as explained in Subsection 1.2.2, the analysis may be focused on the probability for a spike to be fired within a specific time window (Figure 1.8).
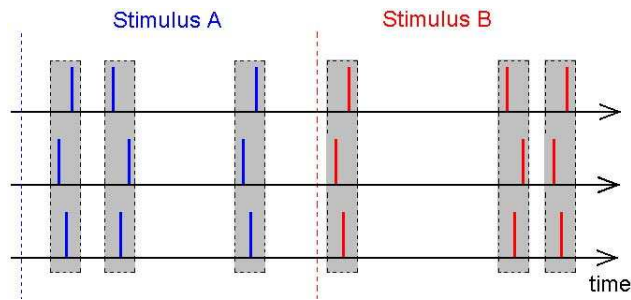
Figure 1.8: Modulation of the time points of spikes fired in response to two different stimuli.

1.2.4 Population code and decoding of stimuli

Several researches have demonstrated that the activity of ganglion cells are strongly correlated among them, i.e. nearby ganglion cells tend to get active together (or inactive together) more often than would be expected by chance (Nirenberg et al., 2001). Particularly, there exists evidence of the concerted and synchronized activity of pairs and groups of ganglion cells under a variety of visual stimuli (Mastronarde, 1989; Meister et al., 1995; Schneidman et al., 2006; Shlens et al., 2006; Pillow et al., 2008). Such evidences have been found due to the use of multielectrode arrays in *in vitro* biological experiments (Taketani and Baudry, 2006) with dissected retinas from different species, which allows to record simultaneously the spikes from populations of ganglion cells in response to diverse visual stimuli. In these experiments, the photoreceptors are stimulated by light patterns whereas the multielectrode array detects the extracellular electrical responses produced by individual ganglion cells (Meister et al., 1994; Berry et al., 1997, 1999; Fernández et al., 2000; Segev et al., 2004; Gunninga et al., 2005).

The retina can be viewed as a neuronal system in which the photoreceptors represent the input of a signal (visual information) and the ganglion cells represent the output of the processed signal (encoded visual information). Hypothetically, if the relationship input/output of a ganglion cells is known, it is possible to determine the code used by the retina to represent any visual scene (Figure 1.9). Therefore, visual stimuli can be reconstructed by computational procedures to decode the spike trains produced by a population of ganglion cells (Bialek et al., 1991; Nirenberg and Latham, 1998). One of the first attempts to decode a time-dependent visual stimulus from the responses of a population of ganglion cells was introduced by Warland et al. (1997). In this work, the authors utilized the isolated retina of a tiger salamander and the stimuli was a spatially uniform field whose intensity varied randomly over time. Subsequently, two decoding strategies (linear reconstruction and artificial neural network) were applied to reconstruct the stimuli. One of the main observations in that work was the influence of the number and type of ganglion cells on the quality of reconstruction of stimuli; the performance of reconstruction improved as more nonredundant cells were included, whereas

inclusion of cells of the same type did not produce evident improvements in the reconstruction. In addition, linear reconstruction was shown to be as effective as the neural network, so most of the information about these stimuli were represented by linear operations on the code. In fact, subsequent studies have demonstrated that the choice of the classification method does not play a relevant role in the reconstruction performance (Nicolelis et al., 1998). Nevertheless, reconstruction methods based on Bayessian classifiers (Zhang et al., 1998; Kass et al., 2005; Winzenborg et al., 2010), linear discriminant analysis (Fernández et al., 2000; Greschner et al., 2006), principal component analysis (Tovée et al., 1993), as well as supervised and non-supervised neural networks (Ferrández et al., 1999) have been widely applied with relative good performance.
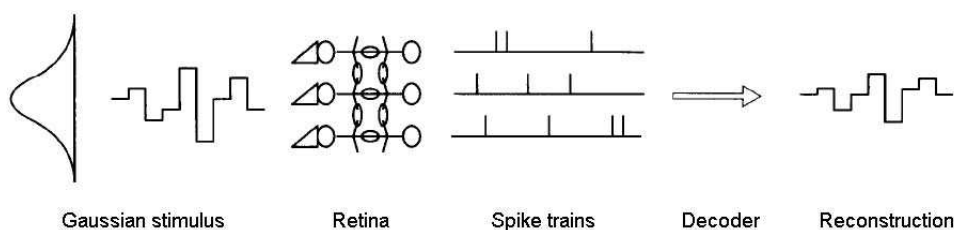
Figure 1.9: Schematic representation of a standard procedure for reconstruction of visual stimuli. A Gaussian distribution of intensities was applied onto the retina and a multielectrode array recorded the spike trains elicited by the ganglion cells. Subsequently, the spike trains were decoded to obtain an estimation of the stimuli. Scheme taken and modified from Warland et al. (1997).

1.3 Saccades and fast decoding of dynamic motion

1.3.1 Saccade movements

The early visual system receives continually natural stimuli that must be encoded by the retina in very short periods of time. The brain in turns decodes at amazing speeds this information, which is a fundamental function for sur-

vival and everyday activities of animals and humans. One of these functions is related with detection and tracking of moving objects and prediction of their future positions. Typical examples include the capacity of an animal to determine how fast must run pursuing its prey according to the velocity that employees to escape; another case is when a person has to determine if the velocity of a vehicle allows him/her to cross a street before it comes. These tasks are performed when the eyeball moves to change the direction of gaze for pursuit of moving objects. Such movements are known as saccades, which allow the dynamic fixation on particular points in the visual scene and definition of details (Yarbus, 1967).

The correct perception of the motion achieved by an object and decoding of its dimensions plays an important role in the cognitive processes such as learning, prediction, attention and selection (Barnes, 2008). These processes influence the capacity of many living organisms to accomplish ocular pursuit of moving objects and bodies, in other words, the skills of the oculomotor system to detect and characterize motions (Robinson, 1965; Lisberger et al., 1987; Pola and Wyatt, 1992; Elstrott et al., 2008; Ilg and Thier, 2008). For instance, ocular pursuit movements maintain smooth eye velocity close to object velocity, reducing retinal image motion and maintaining visual acuity.

Saccades movements are a property shared among the different visual systems in many alive organisms (Land, 1999), they can occur with a frequency around three to four per second (Gollisch, 2009), and the last perception of the image onto the retina is interchanged after each saccade movement. For this reason, the nervous system has little time to process the encoded visual information produced by the retina during the inter-saccadic intervals. Saccades play also an important role in recognition of static images; small changes of direction of gaze occur to scan the whole area of an image perceived by the retina and it keeps the resolution of the static image reconstructed in the brain.

1.3.2 Fast decoding of dynamic motion

Although saccade movements in ocular pursuit may be voluntarily originated by the observer, these can be induced likely without active participation as reflexive movements (Barnes et al., 1987; Barnes, 2008). In this sense, differ-

ent behavioral experiments have been performed to analyze the mechanisms employed by the early visual system for pursuit of moving objects by means of saccadelike stimulation. Depending on some visual parameters, such as the luminance of the target, size, and initial position in the visual field, it has been demonstrated that the onset of smooth target motion evokes pursuits with a range of latency times of 65 to 130 ms (Lisberger and Westbrook, 1985; Lisberger et al., 1987). In other experiments with ramp stimuli (visual pattern at rest moved suddenly with constant acceleration in a fixed direction) it was reported that acceleration of smooth pursuit movements from one velocity to another occurs in about 130 ms (Robinson, 1965). Even neurons in higher visual areas have been shown to produce highly selective responses to visual stimuli in a range between 100 to 150 ms after the onset of a new stimulus (Perrett et al., 1982; Osborne et al., 2004; Ghose and Harrison, 2009).

One approach to evaluate the speed of visual processing in these periods of time was introduced by Thorpe et al. (1996), whose objective was to establish how much time did normal subjects need to identify between two categories of images: pictures containing an animal and pictures without animals; each presentation of the couple of images lasted 20 ms. The results of this research showed that in most of the cases the categories were correctly identified in 150 ms. In other version of the experiment (Kirchner and Thorpe, 2006), subjects identified the two categories making a saccade to the picture that contained the animal. In this occasion, the fastest reliable eye movements were initiated after 120 ms. In another work presented by Schwartz et al. (2007), it was shown that ganglion cells from mouse and tiger salamander retinas produced synchronous burst of spikes fired when sudden changes of direction were detected. These bursts were measured by the peristimulus time histograms (PSTH) from the responses of ganglion cells, which were characterized by presence of activity peaks greater than 10 Hz; these peaks were located in ∼250 ms in salamander retina and ∼190 ms in mouse.

Another approach introduced in analysis of retinal code has been oriented for decoding of motion by use of saccadelike stimulation. Specifically, some researches have tried to determine the role of the ganglion cells from the beginning until the end of a saccade movement. One study in this sense was presented by Roska and Werblin (2003); in this work, authors played shifting

natural movies to observe responses of ganglion cells in rabbit retina during and after saccade movements. They found two types of ganglion cells according to their reaction form: some ganglion cells were inhibited during the saccade and fired bursts of spikes after the saccade ended to encode information of a new moving image; another type of ganglion cells react increasing their activity by means of fired spikes during the saccade in order to encode information while saccade movement is occurring. The authors of this work established that the suppressed activity of some ganglion cells during the saccade could function as a reset of the encoded visual information transmitted from the retina. This mechanism may act as marker of the beginning of a new signal transmission episode (Gollisch, 2009). A similar study developed by Amthor et al. (2005) identified two different behaviors of ganglion cells in rabbit retina by simulation of light change that are likely to occur during a saccade. In this work, authors demonstrated that luminance characteristics of the image played before the saccade affected considerably the responses of ganglion cells to the image played after the saccade. Likely, authors found that outputs of some ganglion cells were suppressed during the saccadelike stimulus, whereas other cells enhanced their responses few hundred milliseconds after the end of the saccade movement.

Archer fish is one of the most interesting case in nature where feeding depends on the ability of an organism to pursue a prey with saccade movements. It is widely known that archer fish can locate an insect prey from its position underwater and shoot it down using powerful jets of water from its mouth. The prior location of its target is normally produced by saccade movements to shift the direction of its gaze. Rossel et al. (2002) reported that archer fish can predict the point on the water where its insect prey will fall only about 100 ms after it shoots it down. This fast prediction allows archer fish to arrive quickly to this point and to devour its prey.

Some previous works have demonstrated the feasibility to estimate motions directly from the relative timings in individual retinal ganglion cells of primates. The basis of the method applied in these studies is that if retinal ganglion cells respond identically, then a response in common should on average be produced in each cell by the time correction of the stimulus onset over each receptive field. The motion is identified by the alignment of spike

trains from the cells after the onset correction expected at the motion. The procedure included the calculation of the cross-correlation between pairwise cells implemented initially by Reichardt (1961) to establish standard models of motion sensing, which were applied by Chichilnisky and Kalmar (2003) and Frechette et al. (2005) to estimate speeds and directions respectively.

Another study about temporally precise spikes after saccadelike stimuli was presented by Greschner et al. (2006). In this work, ON-OFF cells of turtle retina in response to abrupt intensity changes were analyzed; these stimuli were intended to produce specific spike patterns obtained during current saccade eye movements. Two precise types of bursts separated by some ten of milliseconds were registered: in the first burst, latencies decreased monotonically as the contrast increased, whereas latencies in the second burst showed a nonmonotonic dependence on the stimulus, i.e. short latencies for intermediate contrast and long latencies for high and low contrast. This mechanism utilized by subpopulations of ON-OFF ganglion cells were intended to improve the discrimination of different light-intensity transitions. The authors of this study demonstrated also that discrimination of contrasts transitions reached its best performance if both spike count and latencies from the two bursts are evaluated. This is an indication that identification of specific features of a moving object during a saccade movement is impaired when information of the target is transmitted few milliseconds after the saccade movement is over. One study that demonstrated this fact was presented by Segev et al. (2007) by analysis of retinal code registered from ganglion cells of archer fish. Applying changes of light intensity as stimuli, authors found that the best distinction of targets of different sizes was performed in periods inmediatly after saccades, which are normally made by this kind of fish to shift the direction of its gaze for pursuit of its prey.

Since visual information has to cross at least 10 synaptic stages (from photoreceptors until visual responsive neurons in the temporal lobe) in about 100 ms, it has been argued that transmission of encoded visual information based on a single spike per neuron at each stage is totally feasible (Thorpe, 1990). Obviously, the layer of ganglion cells is considered as one of these 10 synaptic stages. Different researches have been focused their studies to decode stimuli taking into account only the information of the first spike (latency) of a

neural response after the onset of a new stimulus. In this sense, a wide number of theoretical works have been published in identification of faces in natural images (Gautrais and Thorpe, 1998; Thorpe and Gautrais, 1998; van Rullen et al., 1998; Thorpe et al., 2001; Delorme and Thorpe, 2001). In an experiment carried out with salamader retina, Gollisch and Meister (2008) demonstrated that latency of first spikes can transmit considerable amounts of information in encoding of images briefly displayed. In this study, the fastest responses were registered from ON-OFF cells whose first spikes were elicited with very high precision timings. Whereas these latency times were well differentiated by about 40 ms according to the displayed image, the number of spikes fired afterward in the bursts kept almost constant regardless the stimulus. Therefore, for the stimuli applied in this study, latency code was more reliable than encoding based on spike count.

Another work to reconstruct motion saccadelike stimuli was presented by Thiel et al. (2007). In this work, a pattern with dark squares on a bright background was moved on an one-dimensional axis varying its speed and direction. Two coding strategies from the spike trains were evaluated: spike count and latency. This information was employed by a Bayesian classifier to reconstruct velocities and velocity transitions of the motion stimuli. The main results of this work indicated that velocities were encoded mainly by spike count in their most stationary periods, whereas velocity transitions were encoded principally by latencies of the responses provoked by abrupt changes of velocities in the stimuli protocol.

1.4 Thesis overview

The present thesis is organized in in five chapters. As can be seen so far, Chapter 1 of Introduction has been dedicated to explain basically some aspects about the the structure of the retina and retinal code. Likewise, a state-of-the-art of researches with saccadelike stimuli and decoding methods has been included. These last considerations have done inherent the necessity for any method of decoding visual stimuli to reconstruct visual scenes in fast and efficient ways, which is the central issue dealt in this thesis. Chapter 2 describes briefly the experiment performed for acquisition and storage of the database

analyzed in the present work, as well as some procedures to preprocess and organize these data. Initially, a multielectrode array was employed to detect the extracellular responses from a retinal ganglion cell population in the isolated retina of a turtle. These responses were produced by stimulation of the retina with a pattern of black points, which moved along a one-dimensional axis with variations of speed and directions. After a spike sorting process, the responses of 107 ganglion cells were separated. The main goal is hence to reconstruct the motion stimuli of the experiment from the information decoded in the spike trains of these cells. Specifically, the stimuli intended to be decoded were velocities and velocity transitions inherent in the stimuli protocol (Section 2.1). Likewise, Section 2.4 deals with the detection of response triggers to be employed as internal reference for estimation of the coding strategies. As mentioned in Section 1.2.2, decoding of stimuli taking into account these internal references may be considered as the most approached method employed by the brain for detection and decoding of new stimuli that arrive into the retina.

Chapter 3 is oriented to determine if systematically selected cells allow to enhance the efficiency of a decoding procedure for visual stimuli. Firstly, this Chapter explains the methods used to evaluate the selectivity of the cells from their responses to the motion stimuli applied in the experiment (Sections 3.2 to 3.6). Such methods evaluated the unicellular selectivity according to the following properties: a) characteristics of their raster plots, b) reliability, c) directionality, e) discriminability and f) transmitted information. After this explanation, it is indicated how the best cells were selected depending of their selectivity to motion assessed by each of the properties above mentioned. With these cells, small sub-populations were constructed and employed for decoding the stimuli by means of a classifier based on linear discriminant analysis, orienting this procedure for classification on a single trial basis. The decoding was accomplished from the temporal information of the first and the second spikes elicited by individual cells when a new stimulus is detected. In other words, the timings of the first and the second spikes were the coding strategies evaluated for reconstruction of motion stimuli using each of the small sub-populations (Section 3.8); it is worth mentioning that the timing of the first spike represents the information of latency. There are two particularities in

the estimation of such coding strategies. The first one is the fact that they were evaluated after the internal triggers detected by the procedure described in Section 2.4, and the second particularity is their estimation within a short time window after the internal triggers, specifically 150 ms having into account the considerations of fast visual detection indicated by Perrett et al. (1982), Osborne et al. (2004) and Ghose and Harrison (2009). In addition, Chapter 3 explains the performance measure employed to assess the classification in Section 3.9. Therefore, velocities and velocity transitions were reconstructed utilizing each of the sub-populations constructed with the cells selected by the methods above mentioned. The results were compared with reconstructions obtained from sub-populations composed by randomly selected cells and it was found that the best method for selection of cells is the one that assess their discriminability properties. Moreover, the probability distributions of the reconstructions between cells selected by discriminability and random cells were shown to be significant separable. For this reason, the analysis accomplished in the following chapters were based on sub-populations constructed with cells selected by discriminability evaluation.

There are three main issues inherent in the Chapter 4. The first one describes the decoding of stimuli in similar way as accomplished for selection of cells in Chapter 3. The difference is that in Chapter 4 the analysis of the coding strategies is expanded to: a) only first spike (latency), b) first spike combined with second spike and c) first and second spikes combined with third spike (Section 4.1), which were likewise estimated in short windows of 150 ms. Evaluation of both second and third spikes is considered as an indirect form to include information of spike count in the classification method. In this way, the idea is to determine if inclusion of fast coding strategies beyond the latency entails improvements if the classification efficiency of velocities and velocity transitions. Additionally, two more performance measures are described in Section 4.3, which assessed separately the performance of the method for prediction of speeds and direction of the motion stimuli. It was found that the temporal information of the second spikes combined with the one of the first spikes provided an improvement in the prediction of velocities; this improvement got even higher when the decoding were accomplished by combination of the temporal information from the first, second and third spikes. A bit

different were the results in the reconstruction of velocity transitions, because the improvement in the classification performance reached by combination of first, second and third spikes was not markedly different from the ones by the combination of only first and second spikes. In any way, it has been clearly observed that the second and third spikes contain information correlated with the spike count and allowed to improve the classification performances beyond the ones reached by only evaluation of latency.

The second issue dealt in Chapter 4 is the improvement of the classification efficiency using sub-populations constructed with different numbers of ganglion cells (Sections 4.2 and 4.4); as expected, the classification performance improved as the number of cells increased. By application of the performance measures explained in Section 4.3, it could be observed that misclassification of directions were more marked in small sub-populations than in large ones. In contrast, there is few differences between classification of speeds in small and in large sub-populations. Furthermore, when the classification efficiency is plotted in function of the increase of cells, it can be observed a kind of saturation or plateau at a intermediate number of cells, which is more evident in the reconstruction of velocities than in reconstruction of velocity transitions. This means that the contribution of cells gradually included in the sub-populations diminished as their number approached to the largest sub-population. This is a first indication that a number of cells less than the total number detected in the experiment (107 cells) can be enough (optimal) for reconstruction of the motion stimuli. Thus, Section 4.6 describes a method to find a more explicit and optimal number of cells, which is accomplished comparing the contribution to enhance the classification efficiency from the largest sub-population with the contributions provided by each of the others sub-populations.

The third and last issue dealt in Chapter 4 is the analysis of the classification method when the time points of the triggers were modified. The idea was to examine how sensitive is the reconstruction method to variations in time of the internal triggers detected by the algorithm. Two procedures were employed in this step. The first one was to introduce delays homogeneously across all the single trials of the responses from individual cells; the second procedure consisted to introduce likely time delays across the trials but generated in a random manner (Section 4.7). It was observed that the homogeneous delaying

of the triggers enhanced the classification of the velocities and diminished the classification of velocity transitions. From analyse published by Winzenborg et al. (2010) using the same database of this thesis, it was observed that most of the information of velocities is encoded by spike count, whereas accelerations and changes of direction are mostly encoded by latencies. Therefore, a possible explanation of the improved classification efficiency for velocities is that the coding strategies may be estimated in more stationary periods of the responses, specifically the second and third spikes (indirect forms to estimate spike count). In contrast, these delayings could deteriorate the information of latency and diminish the reconstruction of velocity transitions. In the case of random delaying of the triggers, the reconstruction of both velocities and velocity transitions were diminished.

Finally, Chapter 5 presents the conclusions of this research. All the calculations in this work were carried out with with the software Matlab® Version 7.2.0.232 (R2006a).

Chapter 2

Experiment

This chapter is dedicated to introduce a brief idea about the experiment performed to acquire the signals of the database analyzed in this thesis, although this experiment is described in detail by Greschner et al. (2002) and Thiel et al. (2007). In addition, this chapter includes also some methods for preprocessing of these signals, which have been likewise presented by Winzenborg et al. (2010). These concepts are important for the comprehension of certain procedures and methods dealt with in the following chapters of this work.

2.1 Electrophysiological recordings

The extracellular recordings from a population of retinal ganglion cells were acquired by *in vitro* stimulation of the dissected retinas of a turtle (*Pseudemys scripta elegans*). The experiment involved the utilization of a multi-electrode array (MEA) of 100 electrodes (Figure 2.1a) inserted from the pigment epithelium side into the layer of retinal ganglion cells. The retina was stimulated with a template that consisted of small black squares placed on a transparent background that moved linearly across the retina at fixed orientation angle with variation of direction and speed (Figure 2.1b). The protocol was controlled by a computer that variated pseudorandomly the presentation of the stimulus velocities (Figure 2.2). The size of the template was large enough to cover all the area of the retina and the stimuli spectrum consisted of nine velocities rep-

resented by $\Omega = \{$-2.5, -1.875, -1.25, - 0.625, 0, 0.625, 1.25, 1.875, 2.5$\}$. Negative velocities indicate leftward motions and each velocity was kept constant during an interval of 500 ms. Motion sequences with this stimuli spectrum were presented during 365 seconds, ensuring that the sequences sampled all velocities. Transitions from one velocity to itself were excluded, in such a form that the experiment presented 72 possible changes or transitions from an initial velocity to a final one; each one of these 72 transitions were presented 10 times in each sequence. The authors conducted the experiment eight times, in such a mode that the final database contained the responses of a population of ganglion cells from eight repeated sequences of the stimuli protocol.

(a)   (b)
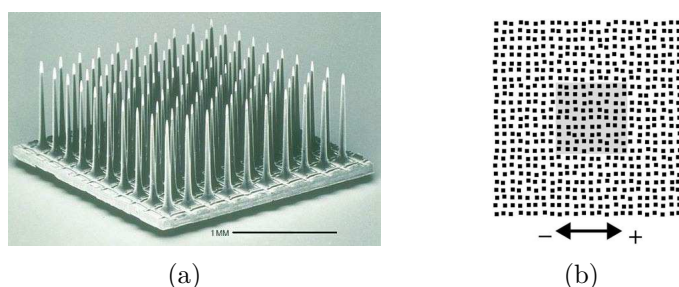
Figure 2.1: (a) Utah 100- electrode array (Cyberkinetics,Foxborough, MA) used to record the response of retinal ganglion cells (Jones et al., 1992). (b) Detail of the spatial random pattern moved along one axis to generate the visual stimuli. The gray square in the center indicates the size of the electrode array. Movement to the right is referred to as positive and movement to the left as negative velocity (modified from Thiel et al. (2007)).

2.2   Spike sorting

It is quite often for a single electrode in this kind of multi-electrode arrays to detect the electrophysiological responses of more than one cell. This situation is not convenient because normally it is necessary to achieve unicellular analysis of the responses measured from a population of ganglion cells. In such cases, a mixture of two or more unicellular responses are present in a single channel of one of the electrodes in the array. For this reason, a spike sorting
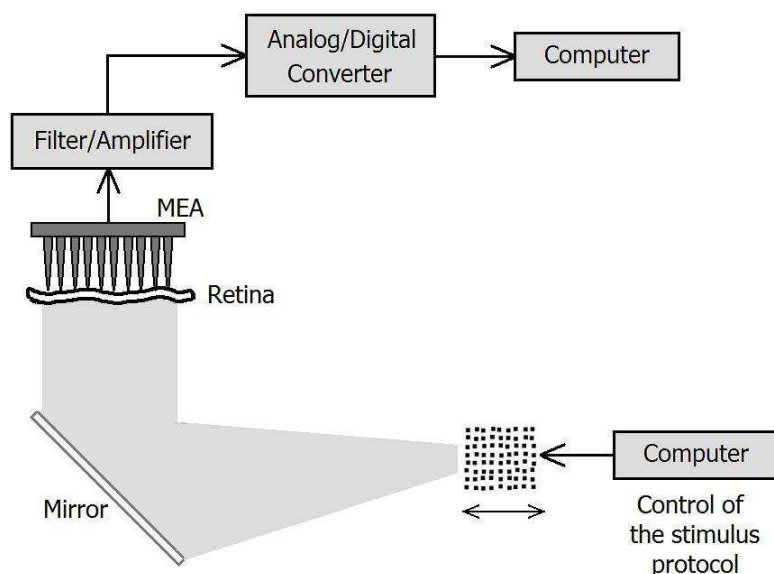
Figure 2.2: Scheme of the setup employed in the experiment.

was performed with the software Spike-Sorter, which is based on a supervised k-means clustering of the individual responses shapes. These procedure separated the extracellular recordings of the multielectrode array into 107 spike trains of individual ganglion cells, whose time points were stored for subsequent analysis. Figure 2.3 shows a stimulus segment of five seconds with the spikes elicited by each cell of the population according to the temporal application of the stimuli.

2.3 Offset correction

Normally, when the transition from a stimulus to another one occurs, there is a time between the instant in which the photoreceptors detect the signals of the new stimulus and the moment in which these processed signals reach the layer of ganglion cells. This time represents a delay that should be compensated for the correct temporal assignment of the retinal responses to the stimuli. In other words, it should be ensured the correspondence of stimuli and responses of ganglion cells in the reconstruction. To compensate this delay, a time shift was introduced into all the time points of the spike trains in the database

25
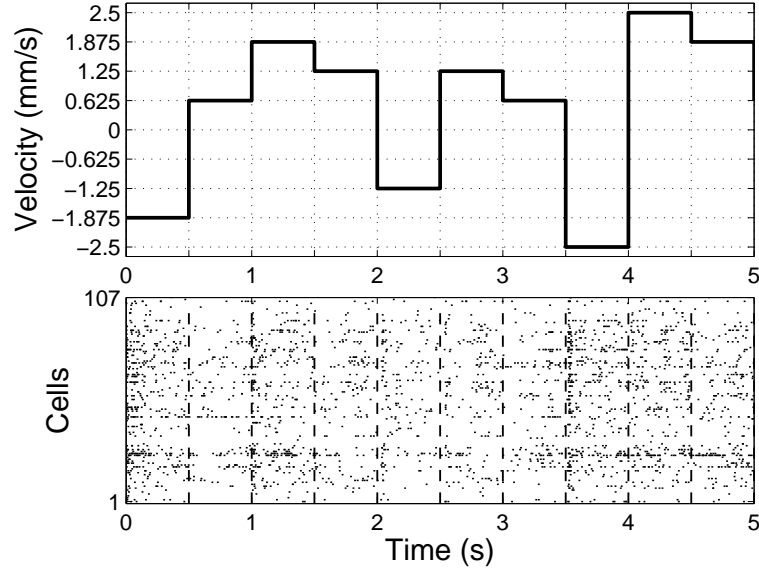
Figure 2.3: Top: five seconds segment of the stimulus protocol with positive and negative velocities indicating motion to the right and left respectively, including the velocity of 0 mm/s as non-motion. Bottom: population raster plot of the spike trains recorded from the retinal ganglion cells.

(Thiel et al., 2007; Winzenborg et al., 2010). The calculation of this time shift consisted initially of the estimation of a post-stimulus time histogram (PSTH) from the spike activity of the 107 pooled ganglion cells with bin sizes of 1 ms. Subsequently, the PSTH of the transitions from 0 to 2.5 mm/s was chosen due to the earliest and strongest responses produced by this specific transition in the activity of the population. To detect the beginning of the activity increase in response to the velocity of 2.5 mm/s, the mean and the standard deviation of the activity before the transitions were calculated for the last 250 ms. In this way, the starting time of the spike population activity was defined as the time in which the population activity exceeded the mean activity plus three times its standard deviation. Finally, the shift time was estimated as the median of the distance between the time in which the population activity began in response to 2.5 mm/s and the time of the transition, which had a value of 56 ms. Hence, this time was subtracted from all the time points of the spikes sorted as mentioned in Section 2.2.
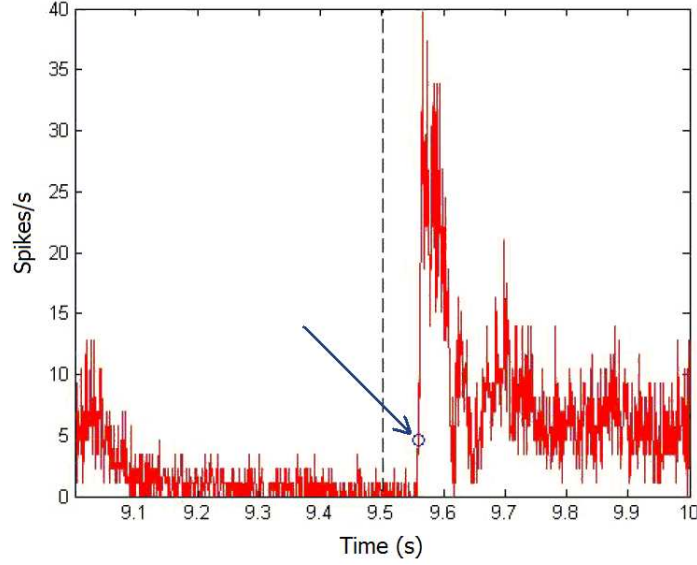
Figure 2.4: Post-stimulus time histogram (PSTH) of the transitions from 0 to 2.5 mm/s. The blue arrow indicates the time in which the population activity exceeded the mean plus three times the standard deviation estimated for velocity 0 mm/s. The vertical dashed line represents the exact time of the transition. This figure has been taken and modified from (Winzenborg, 2007).

2.4   Detection of trigger events

Generally, the brain does not know the exact times in which a new stimulus arrives onto the retina, for which the decoding of the spike trains should be performed relative to internal cues in the nervous system, such as mentioned in Section 1.2.2. In this thesis, an algorithm presented by Winzenborg et al. (2010) was applied for detection of stimulus changes based on the activity of the pooled ganglion cells. This algorithm is based on the concept that strong variations in the activity of the population indicate that a new stimulus have arrived. Hence, the time points in which these variations occur can be employed as relative triggers, from which the features of the retinal code may be estimated and evaluated.

The first step to accomplish the detection of these triggers consisted to calculate a PSTH in similar form as mentioned in Section 2.3. Subsequently, two windows were defined: a large one of 400 ms and a shorter one of

27

45 ms located after the large window. From the spike activity of the population within the large window it was calculated the mean and standard deviation. Additionally, a factor of two standard deviations were added to the mean value for estimation of an upper bound. In the same form, a lower bound was defined subtracting this factor of two standard deviations from the mean of the population activity. In this manner, a trigger was detected when the mean activity of the short window was larger than the upper bound or less than the lower bound. These two windows moved along each of the eight sequences of population activities obtained after the experiment for detection of all the possible triggers. Nonetheless, as a protection against accumulation of triggers, the algorithm did not detect any trigger until 50 ms after the detection of the last one. In the following chapters, the acronym e_t will refer to the triggers detected by means of this method.

Chapter 3

Selection of cells methods and coding strategies

It is reasonable expected that not all the cells recorded in the experiment (Chapter 1) have the capacity to encode motion stimuli. In fact, it has been found that between 30 and 40% of the ganglion cells in the turtle retina are direction selective; most of these cells vary their frequency of fired spikes in function of the speeds inherent in motion stimuli (Bowling, 1980; Ariel and Adolph, 1985; Ammermueller et al., 1995). Hence, it was considered the hypothesis that collection of motion selective cells enables and progressively improves the decoding of the stimuli analyzed in this thesis, whereas the inclusion of randomly selected cells deteriorates the decoding efficiency. To assess this hypothesis, some response properties of the cells (explained from Sections 3.2 to 3.6) were evaluated under the supposition that they reflect the responsivity of the cells to encode motions. In the issues dealt in this chapter, responsivity refers to the covariation between stimulus velocity and firing rate produced by each ganglion cell. Such covariation can be defined as $\partial r/\partial v$, where r denotes the firing rate and v is the stimulus velocity. Subsequently, small hierarchical sub-populations of ganglion cells were constructed with the ranked results of these properties. Finally, the classification efficiency obtained from these sub-populations were compared with those obtained from randomly pooled populations, in order to determine the best method for cells selection.

3.1 Tuning curves of motion selective cells

To explain the fact that not all the neurons detected in the experiment (see Section 2.1) are motion selective, Figure 3.1 shows the tuning curves of latency and spike count of two cells, which do not respond similarly to variations of velocity [1]. To obtain the tuning curves shown in Figure 3.1, the estimations of spike count and latency in each response trial from individual cells was made within the first 150 ms after the detected trigger events (Section 2.4) because behavioral responses are typically observed to occur in times less than 150 ms (Thorpe et al., 1996). The cell whose tuning curves are depicted with the gray lines shows a more defined dynamic range between the slowest and the fastest velocities applied during the stimulation *in vitro* of the retina. In contrast, the cell represented by the black tuning curves responds similarly to all the velocities, which allows to infer that this cell is less selective to motion that the other one.

| (a) Latencies | (b) Spike counts |
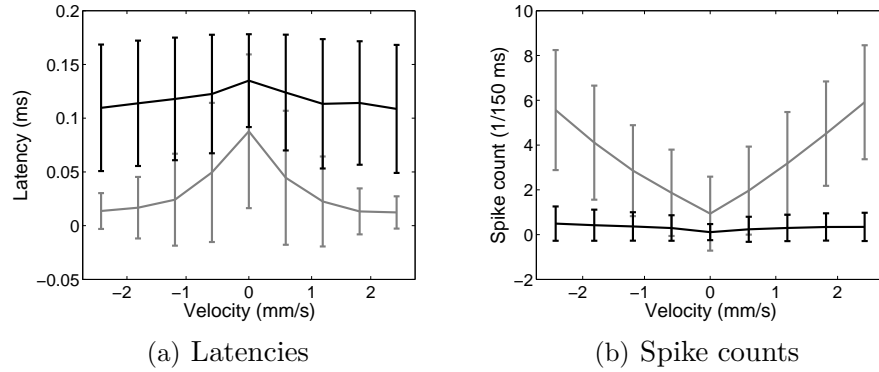
Figure 3.1: Tuning curves of (a) latency and (b) spike count from the responses of two cells to each of the nine velocities of the stimuli spectrum (see Section 2.1). The black line represents a cell with low covariation between its responses and the stimulus velocities, whereas the gray line represents a cell with strong covariation. The mean and standard deviation were determined for 640 stimulus presentations.

---

[1]In the response trials that did no present any spike inside a time window of 150 ms after the trigger, an artificial value of 150 ms was assigned. This situation will be explained in detail in Section 3.8

A set of methods for cells selection are presented in the following subsections. The methods are denominated as follows:

– Visual inspection of raster plots

– Reliability

– Directionality

– Discriminability

– Transmitted information by calculation of Shannon's mutual information

Each of the above mentioned properties was evaluated from the firing patterns of individual cells, notwithstanding the fact that retinal network activity and circuitry can influence the characteristics among their responses. Subsequently, the computed values of each of these properties were ranked in a hierarchical manner together with their respective cells, i.e. from the cells with the highest computed value to the cells with the lowest one.

3.2 Visual selection

This method was applied by visual inspection on the rasters plots generated from the responses of individual cells to every velocity of the stimuli spectrum. The purpose was to look for cells with reliable firing patterns after the onset of the stimulus whose raster plots were produced by 640 presentation of each velocity. This evaluation was made under the assumption that motion selective cells exhibit a noticeable firing activity during the first milliseconds of their responses. Thus, cells that did not present this feature in their raster plots were excluded. Figure 3.2 shows the raster plots of two cells in response to a same velocity; based on this visual assessment 61 cells were selected.

3.3 Reliability

In this method, the reliability of the firing activity of the cells across trials was evaluated during the first milliseconds of their responses after the trigger events

(a) Velocity = 0.625 mm/s   (b) Velocity = 2.5 mm/s
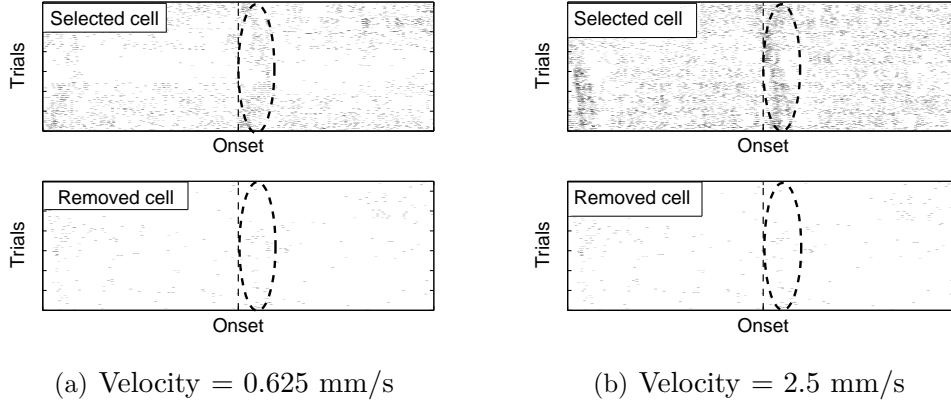
Figure 3.2: Raster plots of two cells with different firing activity in response to two stimulus velocities. The upper panels present the raster plots of a selected cell produced by velocities of 0.625 mm/s and 2.5 mm/s, whereas the lower ones represent the responses to the same velocities of a removed cell. The visual inspection of the firing activity was focused within the dotted line ellipses.

(see Section 2.4). Specifically, it was assumed that the stimulus selectivity is represented by low variability of the spike response to repeated presentations of each velocity (v) from the stimuli spectrum Ω indicated in Section 2.1.

The spike timing reliability of every response's cell was quantified employing a correlation measure proposed by Schreiber et al. (2003). The aim of this procedure is to map every single trial response onto a d-dimensional vector $\vec{\sigma}_i$. Reliability means that all vectors of the trial ensemble point in nearly the same direction in the related d-dimensional space or that the average angle between vector pairs $\vec{\sigma}_i$ and $\vec{\sigma}_j$ is small. Computation of the average cosine then leads to a number which identifies perfect reliability (zero variability) with the value one.

To accomplish the computation of reliability, the spike trains were binned with a time window of 1 ms in the 200 ms following each trigger event. This time was stated under the consideration that, for most of the transitions, the highest firing activity is found in this interval. The bin width, denominated as $\Delta t = 1$ ms, matches the regular time scale of a single spike and defines timing precision. The vector that results from this mapping presents a dimension of $d = 200$, which was convolved with a Gaussian window of mean zero and

standard deviation 5 ms. The final expression of these vectors is given by $\vec{\sigma}_i$, $i = 1, \ldots, n$, where n represents the 640 trials or stimulus repetitions. The spike response reliability Γ was then computed as:

$$\Gamma = \left(\frac{2}{n(n-1)} \sum_{i=1}^{n} \sum_{j=i+1}^{n} \frac{\vec{\sigma}_i \cdot \vec{\sigma}_j}{|\vec{\sigma}_i| \, |\vec{\sigma}_j|} \right). \tag{3.1}$$

Notice that $0 \leq \Gamma$ because all vector components are non-negative. When computing this measure for neurons with different spike rates ($\alpha = \langle k \rangle / (n \Delta t)$ where k denotes the number of ones in a binary sequence) it results obvious that it is biased toward higher spike counts. This bias was corrected by subtracting the average reliability resulting for an ensemble of 640 independent Poissonian spike trains (Figure 3.3). Therefore, the bias-corrected values Γ_c^v
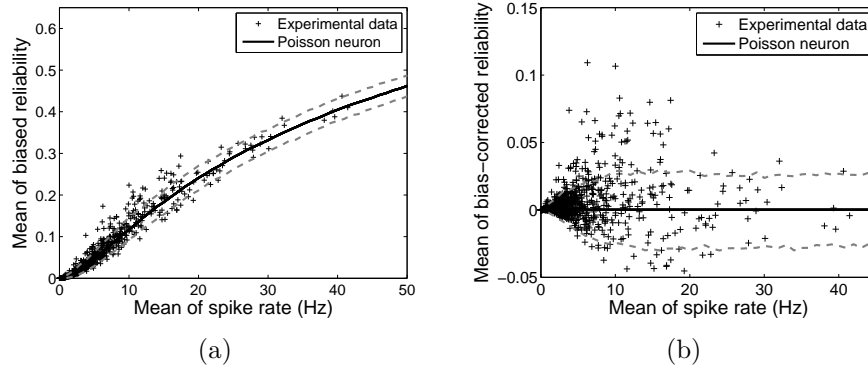
Figure 3.3: The reliability measure (Equation 3.1) is biased toward higher spike rate. This can be seen when simulating 640 independent Poissonian spike trains for a given spike rate and computing the reliability measure. In panel (a) the resulting average is plotted with solid line whereas the dashed lines below and above indicate the 5% and 95% quantiles, respectively. The crosses exemplify the reliability values computed for each of the 107 cells from the spike response to the 640 trials with a specific velocity. In panel (b) we show the same data after bias correction.

were computed for all 107 cells (c) and all 9 stimulus velocities (v). Ranking cells according to Γ for each stimulus separately and comparing the top ten lists showed pronounced differences of *absolute* values. This could be seen as an indication that some stimuli were easier to detect (large Γ_*^v) than others

(small Γ_*^v). In order to pool populations that could handle all tested stimuli comparably, the cells were assessed according to *relative* values γ_c^v, i.e. all absolute values Γ_c^v were normalized to the related maximum as follows:

$$\gamma_c^v = \frac{\Gamma_c^v}{\max_c\{\Gamma_c^v\}} \, . \tag{3.2}$$

To characterize cell c across all velocities, its overall reliability was defined as the average:

$$\gamma_c = \frac{1}{9} \sum_v \gamma_c^v \, . \tag{3.3}$$

The computed mean values of reliability obtained from the responses of each cells are presented in Figure 3.4(a) in form of a hierarchical ranking of cells. Likewise, a scatter plot between the mean of the reliability calculated from each cell and their respective spike count values is shown in Figure 3.4(b). It can be observed that reliability is anti-correlated with the spike rate (correlation coefficient/p-value: $-0.21/0.034$) [2].

(a) (b)

Figure 3.4: (a) Hierarchical presentation of the mean overall reliability values. (b) Scatterplots of mean reliability values vs. average spike rate r_c of each cell. Notice that here the average is performed across trials and all nine velocities.

---

[2] The data of correlation coefficient/p-value presented in this Chapter were calculated by means of the function `corrcoef` of Matlab® Statistics Toolbox

3.4 Directionality

One extension of the considerations from Figures 3.1(a) and 3.1(b) is the selectivity to direction that a cell can exhibit from its firing rate, which should be reflected by their respective tuning curves. The responses of a direction selective cell can produce asymmetric tuning curves, such as observed in Figure 3.5. In this Figure, the asymmetric tuning curves depicted with black lines indicate a selective to leftward motion cell. In this way, directionality is a measure that

(a) Latencies   (b) Spike counts
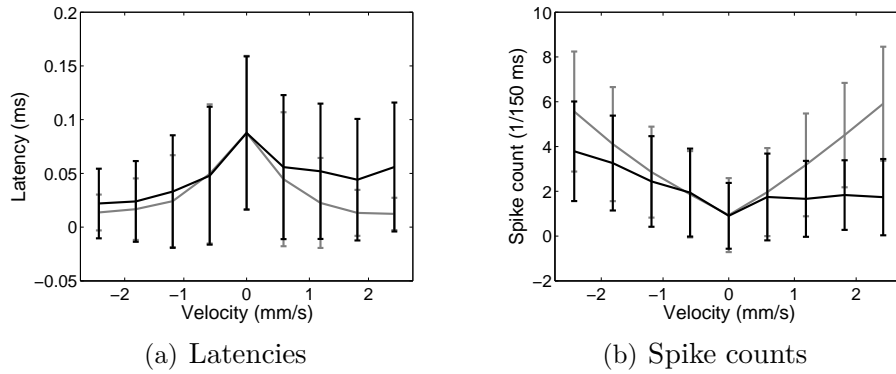
Figure 3.5: Tuning curves of (a) latency and (b) spike count from the responses of two cells to each of the nine velocities of the stimuli spectrum. Both cells present similar values of latency and spike count in response to leftward motion (negative velocities). In contrast, the cell represented by the tuning curves with black lines present lower firing activity and larger latencies for rightward motion. The means and standard deviations were also computed from 640 stimulus presentations.

expresses the asymmetry of the tuning curve of a cell, which was calculated in this case via:

$$\hat{\delta}_c = \frac{\langle \alpha_c^+ \rangle - \langle \alpha_c^- \rangle}{\langle \alpha_c^+ \rangle + \langle \alpha_c^- \rangle} \tag{3.4}$$

where $\langle \alpha_c^+ \rangle$ and $\langle \alpha_c^- \rangle$ are the average spike counts over all rightward and leftward motion respectively [3], i.e.:

$$\langle \alpha_c^+ \rangle = \frac{1}{4} \sum_{v>0} \alpha_c(v) \quad \text{and} \quad \langle \alpha_c^- \rangle = \frac{1}{4} \sum_{v<0} \alpha_c(v) \,. \tag{3.5}$$

Highly left-selective and right-selective cells will yield $\hat{\delta}_c = -1$ and $\hat{\delta}_c = 1$ respectively, while a perfectly symmetric tuning curve (non-direction-selective cell) will result in $\hat{\delta}_c = 0$. Since it is necessary to differentiate only between non-selective and selective to direction cells, regardless of the direction (left or right) for which they are selective, it was considered just the modulus $|\hat{\delta}_c|$. This definition is less stringent than the definition of reliability expressed in Equation 3.1 because it is insensitive to shifting spikes across bins as long as it preserves the total number of spikes. Figure 3.6(a) shows the ranked computed values of directionality from individual cells. Like in the case of reliability (Figure 3.4(b)), directionality is also anti-correlated with the spike rate (correlation coefficient/p-value: $-0.24/0.015$).
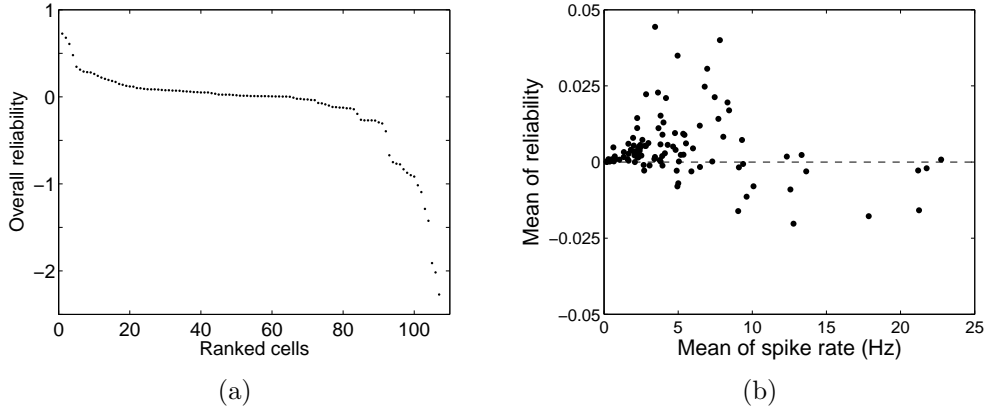

(a)   (b)

Figure 3.6: (a) Hierarchical presentation of the overall directionality values. (b) Scatterplots of directionality values vs. average spike rate r_c of each cell.

---

[3]Here and in the evaluations of discriminability and Shannon's mutual information (Subsections 3.5 and 3.6 respectively), as well as in the evaluation of fast coding strategies (Section 3.8), the calculations were made within the 150 ms following the trigger events (see Section 2.4).

3.5 Discriminability

The measure of discriminability was defined to balance the beneficial effect of responsivity and the detrimental effect of response variability, which is closely related to d' used in signal detection theory (Green and Swet, 1966). In general terms, the discriminability of each cell was computed as the ratio between its responsivity and its response variability, where responsivity and response variability are defined in terms of mean firing rate and standard deviations of firing rate respectively. As in the evaluation of directionality (Subsection 3.4), the discriminability is also insensitive to shifting spikes across bins, since the calculation is performed only from the information of spike counts. To be precise, for each cell c the spike count distribution $p_c(N|v)$ was considered, which describes the probability to observe N spikes of cell c in a time window T and conditioned by the velocity v; its mean and standard deviation are denoted as $\mu_N(v)$ and $\sigma_N(v)$ respectively. Notice that spike counts are related to the tuning curve through division by the length of the counting window T, i.e. $\alpha_c(v) = \mu_N(v)/T$ with T=150 ms. Choosing zero velocity as a reference, the discriminability of velocity v for cell c was computed as:

$$d'_c(v) = \frac{|\mu_N(v) - \mu_N(0)|}{\frac{1}{2}[\sigma_N(v) + \sigma_N(0)]} \, . \tag{3.6}$$

so, the discriminability of each cell c across all velocities was characterized as:

$$d'_c = \max \left\{ \langle d'^+_c \rangle, \langle d'^-_c \rangle \right\} \, , \tag{3.7}$$

where

$$\langle d'^+_c \rangle = \frac{1}{4} \sum_{v>0} d'_c(v) \quad \text{and} \quad \langle d'^-_c \rangle = \frac{1}{4} \sum_{v<0} d'_c(v) \, . \tag{3.8}$$

In contrast to the anti-correlations observed between reliability and directionality with spike rates (Figures 3.4(b) and 3.6(b)), there is a high significant positive correlation between discriminability and spike rate observed in Figure 3.7(b) (correlation coefficient/p-value: $0.55/ \ll 0.001$). In addition, there exists a significant correlation between reliability and discriminability represented in the scatter plot of Figure 3.8 (correlation coefficient/p-value: $0.40/ \ll 0.001$). This fact demonstrates that apart from a large group of cells
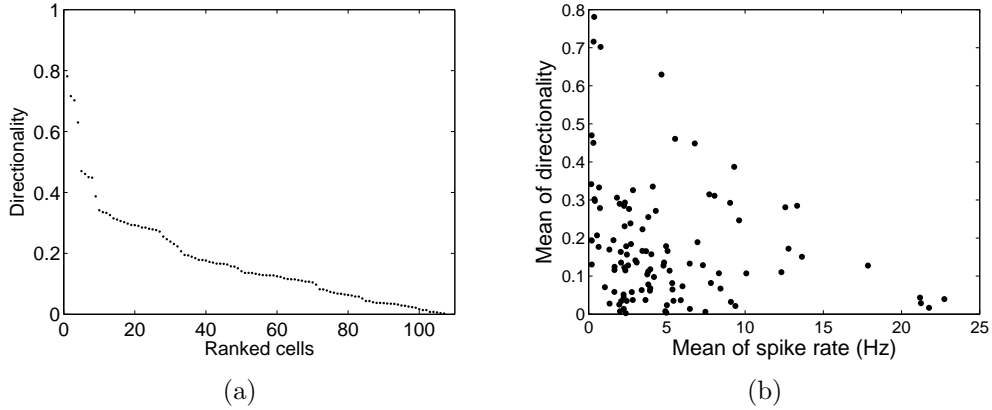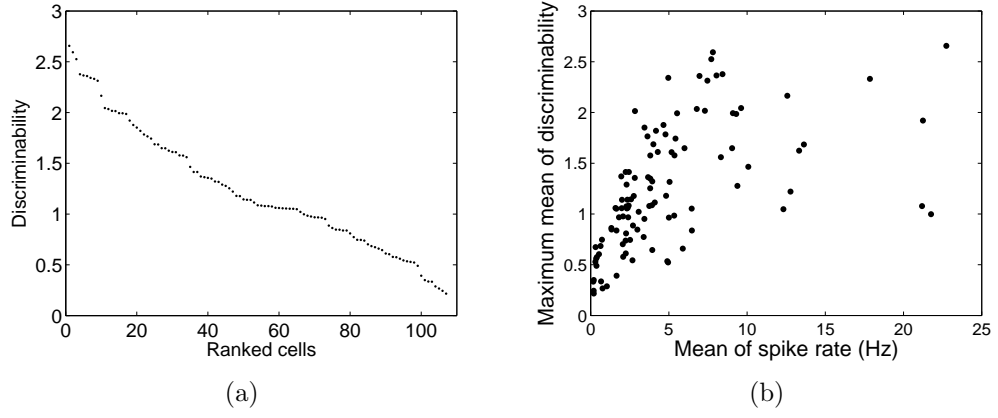
Figure 3.7: (a) Hierarchical presentation of the overall discriminability values. (b) Scatterplots of mean discriminability values vs. average spike rate r_c of each cell.

which, indeed, show a joint increase of discriminability and reliability, there are also a few cells which combine high discriminability with rather low reliability.
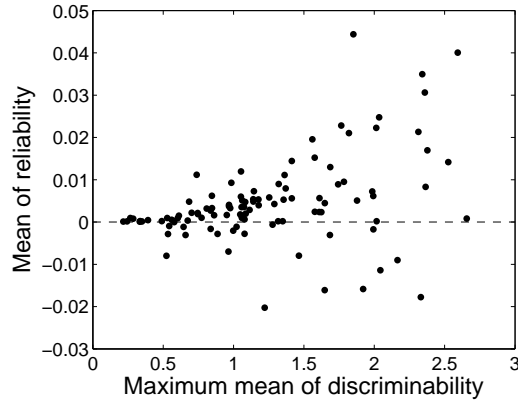
Figure 3.8: Scatter plot indicating a high significant correlation between reliability and discriminability.

3.6 Transmitted information

In this method, the Shannon's mutual information (Brunel and Nadal, 1998; Bonnasse-Gahot and Nadal, 2008; Borst and Theunissen, 1999) was computed from the responses of individual cells according to: spike count, latency and spike timing.

3.6.1 Spike count information

To calculate the information conveyed by spike counts, the number of spikes within the window time of 150 ms after the trigger events was estimated from single trials of individual cells. Subsequently, the Shannon's mutual information (I_c) was computed as follows:

$$I_c(r,v) = \sum_v \sum_r P(v) P(r|v) \log_2 \left(\frac{P(r|v)}{P(r)} \right) \tag{3.9}$$

where $P(s)$ is the prior probability of occurrence of the stimulus velocity v, i.e. 1/9. $P(r|s)$ is the conditional probability of the spike count given by r when a stimulus s is presented and $P(r)$ indicates the probability of the number of spikes fired when any stimulus occurs.

3.6.2 Latency information

The information conveyed by the latency was calculated dividing the time window of the responses from individual ganglion cells into bins of 2, 3, 4, 5, 6, 8 and 10 ms. It was detected the bin that contained the first spike and the Shannon's mutual information was calculated in similar form as indicated in Equation 3.9, in such a way that:

$$I_c(b_{t_1}, v) = \sum_v \sum_r P(v) P(b_{t_1}|v) \log_2 \left(\frac{P(b_{t_1}|v)}{P(b_{t_1})} \right) \tag{3.10}$$

where $P(b_{t_1}|v)$ denotes the conditional probability of the bin that contained the first spike when a stimulus velocity v was presented; $P(v)$ is again the prior probability of occurrence of the stimulus v and $P(b_{t_1})$ denotes the probability of the bin with the first spike given any velocity of the stimuli spectrum.

3.6.3 Spike timing information

The calculation of the information transmitted by the spike timing was also achieved dividing the responses from individual ganglion cells into bins of 2, 3, 4, 5, 6, 8 and 10 ms and estimating the number of spikes in each bin. Regardless of the bin size employed for this calculation, the resulting sequences might cause a huge number of possible responses and problematic calculations of their corresponding probabilities. For instance, sequences with 75 digits are obtained if the bin size is 2 ms. For this reason, the calculation of the Shannon's mutual information for spike timing information is somewhat different compared to the calculations described in Sections 3.6.1 and 3.6.2. In this case, the dimensionality of the responses was initially reduced using a method presented by Foffani and Moxon (2004) for prediction of stimuli. Basically, the method consisted of creating a set of templates based on the peristimulus time histograms (PSTH) with a portion of the collected single-trial responses (training set). Subsequently, the Euclidean distance is calculated between each single-trial of the another portion of data (test set) and every PSTH-templates, in order to predict the stimulus from the spike timing information contained in each trial. The predicted stimulus was assigned to each single trial according to the shortest Euclidean distance between each of them and every PSTH-template, such as proposed by Foffani et al. (2009). In this way, the Shannon's mutual information was computed as follows:

$$I_c\left(\hat{v}, v\right) = \sum_v \sum_{\hat{v}} P\left(v\right) P\left(\hat{v}|v\right) \log_2\left(\frac{P\left(\hat{v}|v\right)}{P\left(\hat{v}\right)}\right) \tag{3.11}$$

where $P\left(\hat{v}|v\right)$ is the probability of predicted velocity $\hat{v}$ when a velocity v is applied, $P(v)$ is the prior probability of occurrence of the velocity v and $P\left(\hat{v}\right)$ is the probability of the predicted velocity $\hat{v}$ regardless the true velocity. The conditional probability $P\left(\hat{v}|v\right)$ was calculated as follows:

$$P\left(\hat{v} = i|v = j\right) = \frac{1}{N} \sum_{t \in j} \left(\min_{v'}\left[X\left(v', t\right)\right] \equiv i\right) \tag{3.12}$$

where

$$X\left(v',t\right) = \begin{cases} \sum_b \left(r_b\left(t\right) - \bar{r}_b\left(v'\right)\right)^2 & v' = j \\ \sum_b \left(r_b\left(t\right) - \left(\bar{r}_b\left(v'\right) - \frac{r_b(t)}{N}\right)\frac{N}{N-1}\right)^2 & v = j, \end{cases} \quad (3.13)$$

N represents the number of trials per stimulus, $t \in j$ indicates the trials corresponding to the velocity $v = j$, the minimum is estimated across all velocities v'; $r_b\left(t\right)$ denotes the single trial response in bin b of trial t, and $\bar{r}_b\left(v'\right)$ is the PSTH-template in the bin b corresponding to the velocity v', which was calculated as:

$$\bar{r}_b\left(v' = k\right) = \frac{1}{N}\sum_{t \in k} r_b\left(t\right) \quad (3.14)$$

To ensure the cross-validation in the prediction of velocities, before the calculation of the Euclidean distance $X\left(v',t\right)$ the single trial response $r_b\left(t\right)$ belonging to stimulus j was removed from the PSTH-template corresponding to stimulus $v' = j$, which is indicated by $\bar{r}_b\left(v'\right)$.
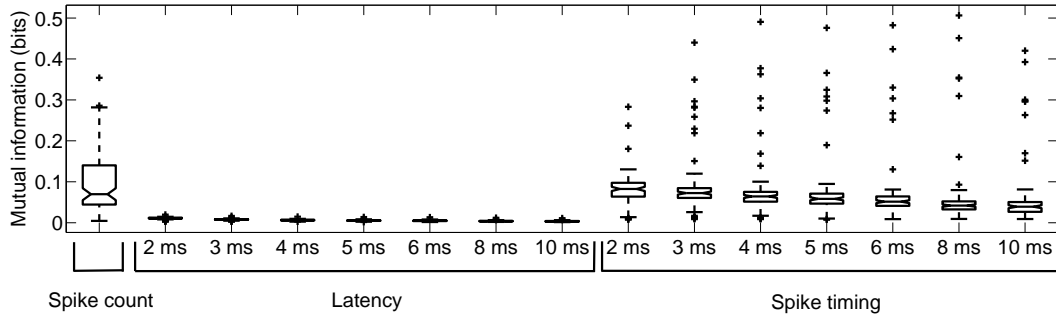
Figure 3.9: Box plots diagrams of the mutual information distributions according to the evaluated properties of the firing patterns (spike count, latency and spike timing); each box plot was constructed with the 107 values of I_c.
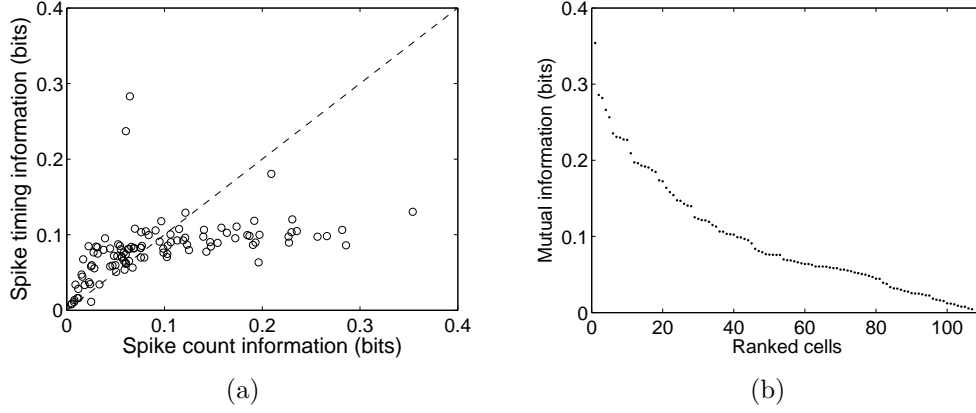
Figure 3.10: (a) Scatterplots of spike timing information vs. spike count information of each cell. In this case, the spike timing information was calculated using a bin size of 2 ms. (b) Hierarchical presentation of the Shannon's mutual information values in bits.

3.7 Construction of sub-populations to choose the best method

In order to determine which of the methods described above (visual inspection, discriminability, directionality, reliability and mutual information) is most efficient for stimulus reconstruction, the top 10 cells from each hierarchical ranking were compiled (Figures 3.4(a), 3.6(a), 3.7(a) and 3.10(b)). In the case of the method based on visual inspection (Section 3.2), it was selected the cells with the best 10 firing patterns observed in their raster plots. Naturally, this procedure is highly subjective to the judgment of the observer. Table 3.1 shows the cell's numbers compiled in each sub-population from the original range of cells (1-107). It can be clearly noticed that ranking with respect to different response features generally yields differently ordered lists. It can be also observed from Table 3.1 that the top 10 of discriminability, reliability and mutual information share various cells among them, whereas the top 10 list of directionality does not share any cell with some of the other three lists.

To determine explicitly the best method for cells selection, the motion stimuli were reconstructed using 10-cells sub-populations constructed with the

Rank	Visual inspection	Discriminability	Reliability	Directionality	Mutual information
1	9	25	79	36	25
2	11	79	61	97	80
3	25	95	52	69	17
4	61	84	9	39	79
5	67	105	24	34	26
6	79	9	17	11	9
7	85	61	95	53	41
8	89	80	1	64	105
9	99	17	99	73	28
10	105	28	41	102	84

Table 3.1: Top 10 lists of the hierarchical ranked cells.

cells of Table 3.1; each sub-population for each of the five methods above explained. This procedure is described in the following Sections.

3.8 Fast coding strategies evaluated

The temporal information of the first two spikes fired by individual ganglion cells in the 10-cells sub-populations was employed to reconstruct the motion stimuli, specifically velocities and velocity transitions. Let n_k^c be the instant in which a spike k is fired by the cell c with $k = \{1, 2, \ldots, K\}$, where K is the number of spikes fired within the first 150 ms of single-trials following the trigger events. The time points of each of the two spikes were computed as follows:

$$t_k^c = \begin{cases} 150 \text{ ms} & n_k^c \in (e_t, \ e_t + 150 \text{ ms}] = \oslash, \\ n_k^c & \text{else} \end{cases} \qquad (3.15)$$

where e_t indicates the trigger events and the subindex k determines the spike assessed (k=1 for the first spike and k=2 for the second spike) [4]. The information of t_2^c was included as an indirect form to evaluate the spike count, due to the correlation between the frequency in the firing activity and the interspike intervals (the shorter the latency, the higher the firing activity and vice versa).

---

[4]Strategy t_1^c is the event-based latency coding already presented by Winzenborg et al. (2010)

If some or both of the spikes k were absent, an artificial value of 150 ms was assigned to t_k^c ($t_k^c \geq 150$ ms), i.e. in cases when the cell c fired the k-th spike outside this time window or when it did not fire any spike during the trial. In principle, this situation could mean lack of information. However, the observation that cell c did not fire a second or even no spike at all in the 150 ms following the trigger event, could indicate valuable information (a missing spike can contribute up to one bit). These data were organized in a matrix as shown in Table 3.2; each row represents a single-trial population response, where T indicates the number of single-trials for each stimulus ($S = \{S_1, S_2, \ldots, S_9\}$ for velocities and $S = \{S_1, S_2, \ldots, S_{72}\}$ for velocity transitions) and each column represents a variable for the stimuli classification (estimations of t_1^c and t_2^c, with $c = 1, 2, \ldots, 10$).

		Cell 1		Cell 2		. . .	Cell 10	
		t_1^1	t_2^1	t_1^2	t_2^2	. . .	t_1^{10}	t_2^{10}
S_1	1 . . . . T			Training set (7 subsequences)				
				Test set (1 subsequence)				
S_2	$T+1$ . . . $2T$			Training set (7 subsequences)				
				Test set (1 subsequence)				
. . .	. . .							
S_N	$(S_N\text{-}1)T+1$ . . . $S_N T$			Training set (7 subsequences)				
				Test set (1 subsequence)				

Table 3.2: Dataset organization for the classification of S_N stimuli, where $N = 9$ for velocities and $N = 72$ for velocity transitions.

Subsequently, the classification of the stimuli (velocities and velocity transitions) was performed using an algorithm based on discriminant analysis included in the function `classify` of Matlab® Statistics Toolbox. This step required the division of the data with a jack-knife procedure into two sets:

training set and test set. The training set consisted of the rows of the matrix corresponding to seven repeated sequences of the experiment, whereas the test set was constructed with the rows belonging to one of the eight repetitions of the experiment (see Section 2.1). This division of the data set guarantees in any classification procedure the cross-validation, i.e. trials employed for testing are not used for training. In this form, the training set was employed by `classify` as input argument to optimally fit the coefficients of a set of linear discriminant equations by maximising the F-ratio between- and within-scatter (see Dunteman (1984, pp. 107-152) and Manly (2004, pp. 105-108)).

Likewise, the operation of `classify` requires for the training set to include the relation between coding elements (in this case the variables t_1^c and t_2^c) and stimuli, whereas in the test set the coding elements are inputs into the discriminant equations previously constructed by `classify`. In this way, one trial of the test set is classified, as much as be possible, inside its corresponding stimulus. To give an idea about this procedure, Equation 3.16 shows the general form of a linear combination of the variables inside a set of discriminant equations for classification of the stimuli in a population of 10 cells:

$$
\begin{aligned}
Z_S \;=\; & W_{S,\,0} + W_{S,\,1}t_1^1 + W_{S,\,2}t_1^2 + \ldots + W_{S,\,10}t_1^{10} \\
& + W_{S,\,11}t_2^1 + W_{S,\,12}t_2^2 + \ldots + W_{S,\,20}t_2^{10},
\end{aligned}
\tag{3.16}
$$

where the terms $W_{S,\,1}$, $W_{S,\,2}, \ldots, W_{S,\,20}$ represent the optimally fitted discriminant coefficients and $W_{S,\,0}$ is a constant for each stimulus. A stimulus is hence successfully classified by Z_S if the mean value of its variables differs considerably from the variables of the other stimuli. In a case like the one presented in this work, in which there are more than two stimuli to reconstruct, it is possible to construct several linear combinations of variables for separation of stimuli. In general terms, if there are S stimuli, S-1 discriminant functions can be computed, which are uncorrelated among them. So, the first function of the set given by Equation 3.16 can be broken down as:

$$
\begin{aligned}
Z_1 \;=\; & W_{1,\,0} + W_{1,\,1}t_1^1 + W_{1,\,2}t_1^2 + \ldots + W_{1,\,10}t_1^{10} \\
& + W_{1,\,11}t_2^1 + W_{1,\,12}t_2^2 + \ldots + W_{1,\,20}t_2^{10},
\end{aligned}
\qquad (3.17)
$$

which, returns the maximum possible difference between stimuli. The second one,

$$
\begin{aligned}
Z_2 \;=\; & W_{2,\,0} + W_{2,\,1}t_1^1 + W_{2,\,2}t_1^2 + \ldots + W_{2,\,10}t_1^{10} \\
& + W_{2,\,11}t_2^1 + W_{2,\,12}t_2^2 + \ldots + W_{2,\,20}t_2^{10}
\end{aligned}
\qquad (3.18)
$$

detects as much as possible differences of the stimulus that are not exhibited by Z_1; Z_3 reflects as much as possible of the group differences not displayed by Z_1 and Z_2; and so on. Ideally, the first few functions may be enough to represent all the important differences among the stimuli (Fernández et al., 2000; Greschner et al., 2006). Therefore, each single index Z_S compiles the information contained in the variables t_1^c and t_2^c, setting the basis to assign features estimated from each single-trial to its respective stimulus. In this way, the information of each single-trial of the test set, given by the estimated data from t_1^c and t_2^c, is assigned to the stimulus S providing the largest discriminant Z_S of all the stimuli. The repeated sequences of the experiment were permuted eight times to construct different training and test sets. This procedure for classification of the stimuli was accomplished for all the 10-cells sub-populations constructed as explained in Section 3.7.

3.9 Evaluation of the performance of reconstruction

The performance of the reconstruction accomplished by linear discriminant analysis was evaluated comparing the estimated and true stimuli (velocities and velocity transitions). Initially, it is described in the present Section the percentage of correctly estimated stimuli, which is denoted as E^P in Equa-

tion 3.19 [5],

$$E^P(N) = \frac{100}{|T_{test}|} \sum_{t \in T_{test}} \delta\left(\hat{s}(t) - s\left(t\right)\right), \tag{3.19}$$

where $|T_{test}|$ is the size of the test set and δ is the delta function ($\delta(0) = 1$ and 0 otherwise). With the aim to determine if the systematic cells selection produces better classification efficiency, the stimuli were reconstructed using 100 sub-populations composed by 10 randomly selected cells each. The results of the classification efficiency for velocities and velocity transitions, measured by Equation 3.19, are presented in form of box-plots in Figure 3.11. Each box plot was constructed with eight values of E^P due to the eight permutations of training and test sets, except for the estimations obtained from the sub-populations constructed with random cells. In this last case, a mean of the E^P values was calculated from each of the 100 sub-populations; these means were in turn averaged to obtain the data used in the construction of the box-plots for sub-populations with randomly selected cells.

It can be observed in the plots of Figure 3.11 that the median values obtained from evaluation of discriminability are larger than those obtained with the other methods. To accomplish a more explicit comparison among them, an evaluation of pairs was made using an ANOVA test and posthoc 5% hsd-test (also known as Tukey-Kramer test) included in the function `multcompare` of Matlab® Statistics Toolbox. Basically, this function returns a matrix of pairwise comparison results with information about which pairs of distributions are significantly different and which are not. An ordinary t-test was not applied in order to avoid that the confidence level value be applied to each comparison. In this last situation, the chance of incorrectly finding a significant difference would increase with the number of comparisons. Therefore, a multiple comparison procedure provides an upper bound on the probability that any comparison will be incorrectly found significant. The procedure to compare the distributions showed in Figure 3.11 was performed with a confi-

---

[5]Two more performance measures were calculated: absolute error of the speeds reconstruction (E^S) and percentages of correct estimated directions (E^D). These measures will be explained in Section 4.3 when it is described the reconstruction of stimuli with variations of the number of cells in the population. The three performance measures (E^P, E^S and E^D) were previously applied in the work presented by Winzenborg et al. (2010)
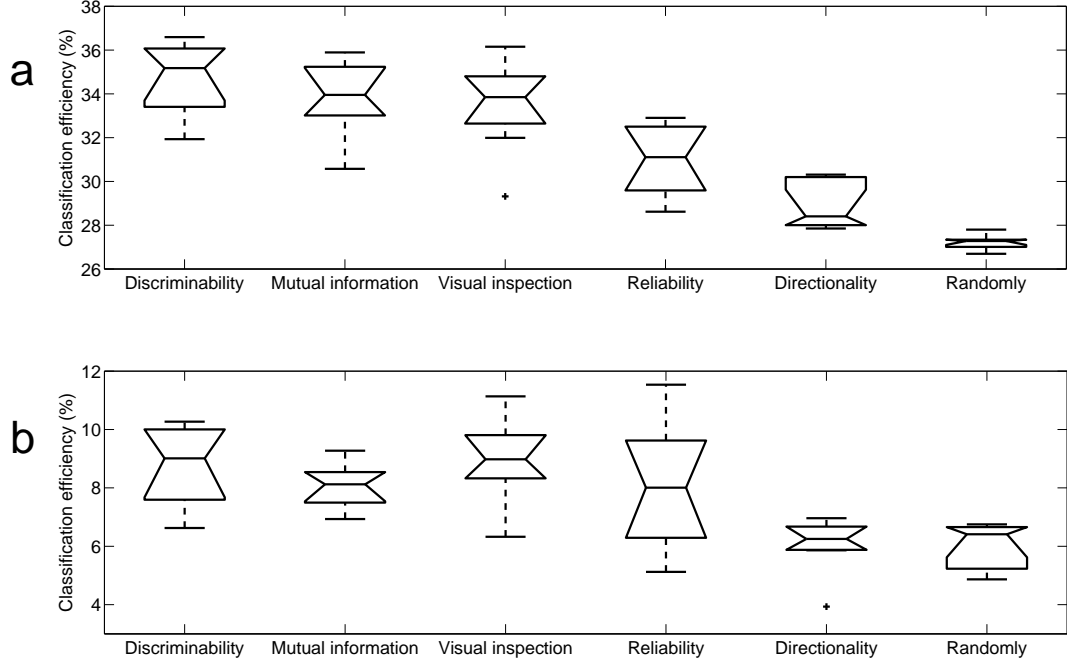
Figure 3.11: Box plots diagrams for reconstruction of velocities (a) and velocity transitions (b) using 10-cells sub-populations and evaluating the properties of their firing patterns.

dence level of 0.005.

Table 3.3 contains the output of this multiple comparison performed by `multcompare`, which is formed by three main columns; the first one contains the pairs of distributions whose comparisons are tested; these distributions are the same showed in the box plots of Figure 3.11. The second column contains three sub-columns that represents the differences between the distributions compared for reconstruction of velocities. Specifically, the values in the second sub-column are the results when the means of the second distributions were subtracted from the means of the first ones, whereas the first and third sub-columns contain the bounds of 95% confidence intervals for the true means. If the confidence interval does not contain 0.0, then the difference between distributions is significant at the 0.05 level. The information in the third main

column is the same of the second column but for reconstruction of velocity transitions.

Compared groups		Velocities			Velocity transition		
Discriminability	Mutual information	**-1.44**	**0.86**	**3.17**	**-1.32**	**0.69**	**2.72**
Discriminability	Visual inspection	**-1.08**	**1.22**	**3.53**	**-2.21**	**-0.19**	**1.82**
Discriminability	Reliability	1.42	3.73	6.04	**-1.31**	**0.70**	**2.72**
Discriminability	Directionality	3.49	5.80	8.11	0.67	2.70	4.72
Discriminability	Random	5.19	7.50	9.81	0.71	2.73	4.75
Mutual information	Visual inspection	**-1.95**	**0.35**	**2.66**	**-2.91**	**-0.89**	**1.12**
Mutual information	Reliability	0.55	2.86	5.17	**-2.01**	**0.00**	**2.02**
Mutual information	Directionality	2.62	4.93	7.24	**-0.01**	**2.00**	**4.02**
Mutual information	Random	4.32	6.63	8.94	0.01	2.03	4.06
Visual inspection	Reliability	0.20	2.51	4.82	**-1.12**	**0.89**	**2.92**
Visual inspection	Directionality	2.27	4.58	6.89	0.87	2.89	4.92
Visual inspection	Random	3.97	6.28	8.59	0.91	2.93	4.95
Reliability	Directionality	**-0.24**	**2.06**	**4.37**	**-0.02**	**1.99**	**4.02**
Reliability	Random	1.46	3.77	6.08	0.01	2.03	4.05
Directionality	Random	**-0.60**	**1.70**	**4.01**	**-1.98**	**0.03**	**2.05**

Table 3.3: Results of the multiple comparisons for classification of velocities and velocity transitions. The comparisons that are not significantly different are represented by values marked with bold.

Based on the observations from Figure 3.11 and Table 3.3, it was determined that the cells selected by discriminability (see section 3.5) offer the best reconstruction performance. Therefore, the posterior analysis will be performed with the cells ranked by means of this method.

Chapter 4

Reconstruction performance vs population size

This chapter is dedicated to describe the procedure to reconstruct the motion stimuli (velocities and velocity transitions) based on the information transmitted by only three spikes in varying population sizes. These sub-populations were constructed from the cells ranked by their discriminability (Figure 3.7(a)), due to their tendency to provide the best classification performance for sub-populations of 10 cells (Section 3.5). For this analysis, the number of ganglion cells included in each sub-population covered a range between 5 and 100 cells with increases of 5 cells, so the decoding of the signals is carried out in 20 different sub-populations of ganglion cells. This last issue will be explained in detail in Section 4.4.

4.1   Coding strategies

The reconstruction of visual motion was performed evaluating fast coding strategies in a similar form as explained in Section 3.8 from individual cells of each sub-populations. Nevertheless, in this analysis the reconstruction was performed including the temporal information from the third spike fired by individual cells (t_3^c) within the defined time window of 150 ms following the trigger event (see Section 2.4). The estimation of t_3^c was included in the analysis under the assumption that it is an additional indirect form to obtain

information about the spike count. Likewise, t_3^c was estimated according to the Equation 3.15, which has been applied for the first and second spikes, denoted as t_1^c (latency) and t_2^c respectively. Hence, three coding strategies were defined, which are summarized in Table 4.1.

Coding strategy's acronym	Description
t_1	t_1^c
$t_1\&t_2$	t_1^c combined with t_2^c
$t_1\&t_2\&t_3$	t_1^c combined with t_2^c and t_3^c

Table 4.1: Coding strategies evaluated in the reconstruction of motions stimuli

It is worth to notice that the second coding strategy ($t_1\&t_2$) of the above mentioned Table, had been already evaluated to determine the best method for selection of cells in Section 3.8. Comparisons of t_1 with strategies $t_1\&t_2$ and $t_1\&t_2\&t_3$ allows to assess the improvements in reconstruction efficiency when the temporal information of one or two more spikes are included in the analysis. The classification of the motion stimuli (velocities and velocity transitions) was accomplished in similar form as described in Section 3.8, i.e. using an algorithm based on discriminant analysis included in the function `classify` of Matlab® Statistics Toolbox. Likewise, the data were organized in similar form as shown in Table 3.2. Table 4.2 represents the matrix when the classification was accomplished by evaluation of the coding strategy $t_1\&t_2\&t_3$. Naturally, classification of stimuli evaluating only t_1 or $t_1\&t_2$ entailed the remotion of the columns t_2^c and t_3^c according to the case.

4.2 Estimated velocities vs. true velocities

A first approach to evaluate the performance of the reconstruction of velocities is shown in the four matrices of Figure 4.1. It can be identified in each matrix an ascending diagonal from the lower left corner to the upper right one; each of the patches that form this diagonal represents a pair of one actual velocity and the probability that it has been reconstructed correctly. The gray scale establishes that the darker each patch on this diagonal, the higher probability to predict correctly the velocity located in this indice of the matrix (black =

			Cell 1			Cell 2			. . .	Cell N		
			t_1^1	t_2^1	t_3^1	t_1^2	t_2^2	t_3^2	. . .	t_1^N	t_2^N	t_3^N
S_1	1 . . . . T					Training set (7 subsequences)						
						Test set (1 subsequence)						
S_2	$T{+}1$ . . . $2T$					Training set (7 subsequences)						
						Test set (1 subsequence)						
. . .	. . .											
S_N	$(S_N\text{-}1)T{+}1$ . . . $S_N T$					Training set (7 subsequences)						
						Test set (1 subsequence)						

Table 4.2: Dataset organization for the classification of the stimuli by evaluation of the coding strategy $t_1\&t_2\&t_3$ in a sub-population with N ganglion cells

100%, white $= 0\%$). The matrixes in turn are organized in two columns and two lines. A comparison between both columns allows to assess visually the effect of changing between two coding strategies: t_1 (left panels) and $t_1\&t_2\&t_3$ (right panels). In contrast, a comparison between both lines shows the effect of using a large sub-population composed of 100 cells (top panels) vs. a smaller sub-population with 5 cells (bottom panels). According to the observations of each matrix, the tendency to correctly classify the velocities is more evident when the velocities were reconstructed with large sub-populations. In addition, adjacent reconstructions on the diagonal can be observed, indicating slight differences (higher or lower) of the reconstructed speeds compared to the true speeds.

Furthermore, it can be observed an off-diagonal from the left upper corner until the lower left one of each plot, which is more accentuated in the reconstructions using 5 cells; this off-diagonal indicates velocities whose speeds have been correctly classified (or slightly misclassified) but not their directions. The

(a) t_1 100 cells

(b) $t_1\&t_2\&t_3$ 100 cells

(c) t_1 5 cells

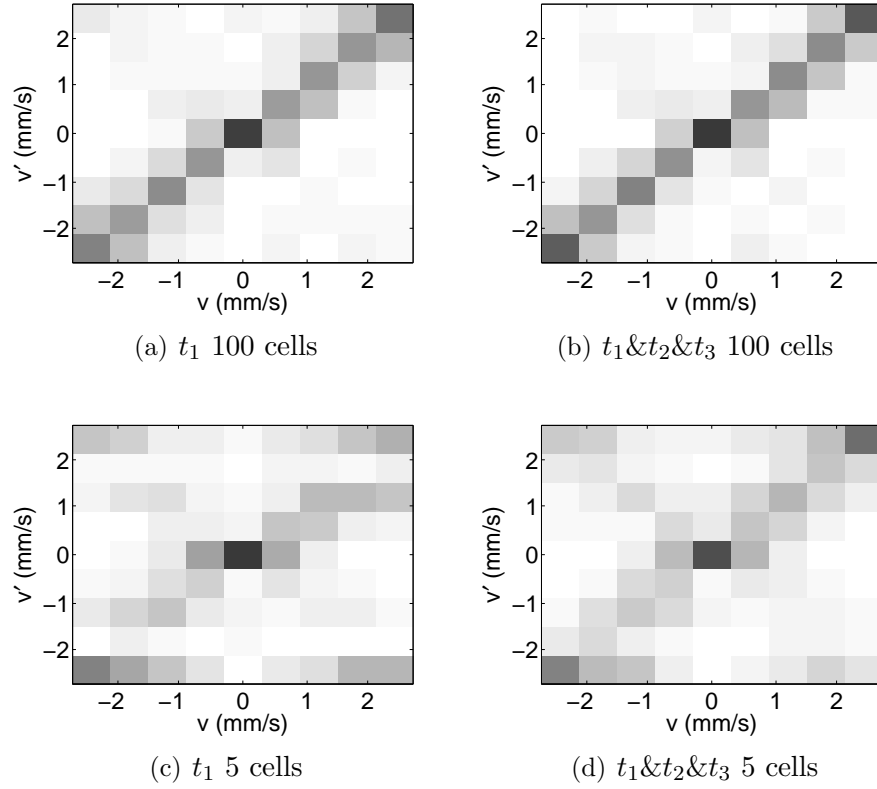(d) $t_1\&t_2\&t_3$ 5 cells

Figure 4.1: Graphical representation of velocity reconstruction with true velocities ordered along the abscissa (v) and reconstructed velocities along the ordinate ($v\prime$). Since the stimulus protocol guaranteed that all velocities occurred with equal frequency the gray values within a matrix column should sum up to a constant.

observation of Figure 4.1 suggests difficulties to predict correctly direction of motion in small sub-populations regardless of the coding strategy evaluated. This fact causes a diminished reconstruction performance for sub-populations constructed with few cells, even when they are top-ranked cells. Another detail observed in the plots of Figure 4.1 is the high probability to classify correctly the velocity of 0 mm/s. This situation may be explained on the basis that the cells fire very few spikes in 150 ms when the velocity stimulus is 0 mm/s, for which the artificial value of 150 ms is assigned in a high proportion to the variables t_1^c, t_2^c and t_3^c allowing a better accuracy in the prediction of this velocity. Additionally, it is likely to find cases in which slow speeds are misclassified as 0 mm/s and vice versa. Deviations in the classification of speeds and misclassification of directions are analyzed in detail by calculation of additional performance measures: absolute error and percentage correct estimated directions, which will be described in Section 4.3.

4.3 Additional performance measures

4.3.1 Absolute error of speeds reconstruction

As can be noticed, deviations in the prediction of speed and misclassification of direction do not have influence on the calculation of the percentages of correct estimation, which has been expressed by Equation 3.19. Therefore, one of the additional performance measures included in this thesis evaluates the possible misclassification of speeds based on their mean absolute error expressed by Equation 4.1:

$$E^S(N) = \frac{1}{\text{chance}} \frac{1}{|T_{test}|} \sum_{t \in T_{test}} |\hat{s}(t) - s(t)|, \qquad (4.1)$$

where

$$\text{chance} = \frac{1}{|\Omega|^2} \sum_{\theta \in \Omega} \sum_{\theta' \in \Omega} |\theta - \theta'|, \qquad (4.2)$$

In case of the expression given by Equation 4.2, N is the size of the population and Ω is the stimuli spectrum that had been indicated in Section 2.1.

4.3.2 Percentages of correct estimated directions

The performance of the method of reconstruction for estimation of the motion directions was evaluated by:

$$E^D(N) = \frac{100}{|T_{test}|} \sum_{t \in T_{test}} \delta \left(signum\left(\hat{s}\left(t\right)\right) - signum\left(s\left(t\right)\right)\right) \qquad (4.3)$$

where

$$signum(a) = \begin{cases} 1 & a > 0 \\ 0 & a = 0 \\ -1 & a < 0 \end{cases} \qquad (4.4)$$

4.4 Reconstruction of stimuli

4.4.1 Reconstruction of velocities vs. number of cells

The performance in the reconstruction of velocities according to the size of the sub-populations (N) and coding strategies evaluated is analyzed in Figure 4.2 [1]. In principle, it is evident that the values of correct estimations are always above the chance level for every coding strategy evaluated and population size. In this case, the chance level is $1/9 = 0.11$ or 11.11% (dotted line) because the nine velocities of the stimulus protocol. From Figure 4.2a it can be observed that the larger sub-population, the higher percentage of correct estimation (E^P), although when the sub-populations get a size greater than about 40 cells there exists a saturation in the values of E^P. The decoding of the velocities evaluating only the temporal information of the first spike (t_1 indicated with the gray line) is sufficient to reach percentages of correct estimation, whose mean values vary between $\sim 27\%$ (for the smallest sub-population constructed with 5 cells) and $\sim 46\%$ (for the greatest sub-population constructed with 100 cells). It can be also observed that the performance of classification was

---

[1]Here and in the following figures that show the results of classification, the values of mean and standard deviations were determined by permutation of training and test sets from the eight repeated sequences of the experiment, such as explained in Section 2.1. In addition, the location of these points over the curves are slightly shifted to avoid possible horizontal overlapping of the standard deviation bars between them.

systematically improved when the temporal information of the second and third spikes were included in the analysis (t_1&t_2&t_3 indicated with the black line); in this case, the mean values of E^P variates between ~ 31 and $\sim 49\%$, for the smallest and the greatest sub-populations respectively. It can be also noticed that the standard deviation bars in Figure 4.2a are not overlapped among them when the sub-populations contain less than 80 cells. Moreover, the saturation in sub-populations with more than 40 cells coincides with a reduction of the standard deviation values of E^P, which hold specially for the sub-populations of 45, 50 and 55 cells. Figure 4.2b shows the differences ($\Delta E^P(N)$) between the improvement reached when t_2 and t_3 were also included for the classification (gray line) in contrast with the improvement including only t_2 (black line) [2]. These differences were calculated in terms of the absolute improvements and in function of the size of the sub-populations (N) as follow:

$$\Delta E^P_{t_1\&t_2\&t_3-t_1}(N) = \overline{E^P_{t_1\&t_2\&t_3}(N)} - \overline{E^P_{t_1}(N)} \tag{4.5}$$

$$\Delta E^P_{t_1\&t_2-t_1}(N) = \overline{E^P_{t_1\&t_2}(N)} - \overline{E^P_{t_1}(N)} \tag{4.6}$$

where $\overline{E^P_{t_1\&t_2\&t_3}(N)}$ indicates the mean values from the percentages of correct estimation (E^P) by evaluation of t_1&t_2&t_3. In similar form, the meanings of both $\overline{E^P_{t_1\&t_2}(N)}$ and $\overline{E^P_{t_1}(N)}$ can be inferred as the mean values of E^P by evaluation of t_1&t_2 and t_1 respectively. It can be noticed an enhancement in the classification provided by inclusion of both t_2 and t_3 to t_1, which is reflected in a profit ($\Delta E^P_{t_1\&t_2\&t_3-t_1}(N)$) of $\sim 4\%$. In contrast, the improvement gained when only t_2 is evaluated together with t_1 ($\Delta E^P_{t_1\&t_2-t_1}(N)$) is minor, reaching differences not larger than 3%. Both curves are characterized by a peak when the sub-population has a size (N) about 40 cells and descend systematically as the number of cells increases. This fact is caused probably because larger sub-populations contain a high number of cells whose values of t_2^c and t_3^c were estimated as the artificial value of 150 ms (see Section 3.8). Thus, this situation may entail a poor benefit in the performance of classification as more cell are

---

[2]Notice that the legend of the Figure 4.2b is different from the one of Figures 4.2a and 4.2c. A similar situation arises in Figure 4.3b

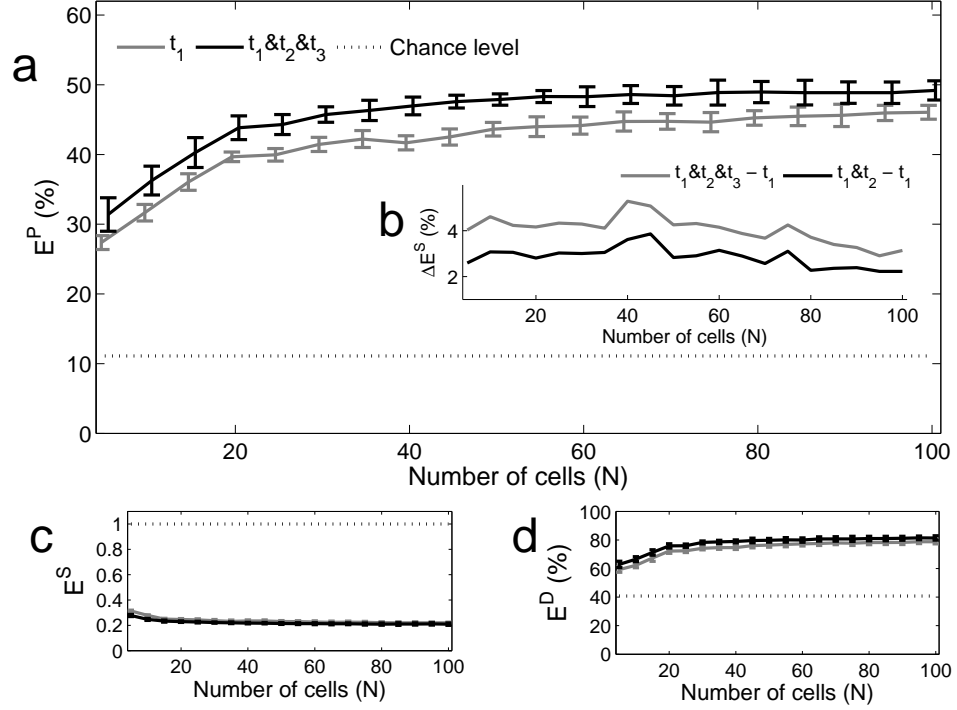included in the analysis, which will be explained more in detail in Section 4.6.

Figure 4.2: Results of performance measures for classification of velocities. a) Percentages of correct estimation (E^P). b) Differences of classification between inclusion of t_2 and t_3 to t_1 and inclusion of only t_2 (see text). c) Absolute error from the classification of speeds (E^S). d) Percentages of correct estimation in the classification of directions (E^D).

Separately in Figures 4.2c and 4.2d the misclassification in the classification of speeds and directions are analyzed, depicting the absolute errors for speed estimation (E^S) and the percentages of directions correctly classified (E^D). From Figure 4.2c it can be observed that the correct prediction of speeds does not seem to be better in large sub-population than in small ones. In this sense, it is expected that the absolute error measure (E^S) decreases whereas percentages of correct estimation of velocities (E^P) and directions (E^D) increases. Just a slight difference in the prediction of speeds can be noticed for sub-populations constructed with less than 15 cells, so the absolute error gets a value of ~ 0.3 for the smallest sub-population and ~ 0.2 for the

largest one regardless the coding strategy evaluated. In contrast, Figure 4.2d shows that when the smallest sub-populations augmented their size to more than 20 cells, the prediction of directions increased from $\sim 60\%$ to $\sim 80\%$. By this obervation it may be inferred that failures of correct estimation in small sub-populations are caused possibly by lack of direction selective cells, such as suggested in the analysis of the plots of Figure 4.1. Additionally, neither in Figure 4.2c nor in Figure 4.2d there are clear signs that classification by evaluation of the coding strategy $t_1 \& t_2 \& t_3$ is better than the one accomplished by only t_1. Another particular situation in these two Figures is that the standard deviation bars got shorter in comparison to the ones of Figure 4.2a. This fact can be explained because the statistical data to train the classifier augmented when speeds and directions were reconstructed separately. In any case, the saturations of the results observed in sub-populations with more than 40 cells is evident for all the performance measures (E^P, E^S and E^D) and are sufficiently far from their respective chance levels.

4.4.2 Reconstruction of velocity transitions vs. number of cells

In addition to the reconstruction of the velocities, the coding strategies were also evaluated to reconstruct velocity transitions. The purpose of this step is to assess the capacity of the coding strategies to transmit information of certain characteristics of motion given by acceleration, deceleration and sudden changes of direction. In this study, the reconstruction of velocity transitions involves the simultaneous prediction of the velocities before and after the trigger event that detects the arrival of a new stimulus (see Section 2.4). The coding strategies employed were the same evaluated for reconstruction of velocities and indicated in Table 4.1 and the results are presented in similar form like in Figure 4.2.

Figure 4.3a shows the enhancement in the percentages of correct estimation (E^P) as the size of the sub-populations (N) increases, which are likewise located always above the chance level for every coding strategy evaluated and population size. In this case, the chance level is $1/72 = 0.014$ or 1.4% (dotted line) because the 72 velocity transitions of the stimulus protocol. By eval-

uation of the coding strategy t_1 (gray line), the mean values of E^P variates between $\sim 4.9\%$ for the smallest sub-population (5 cells) and $\sim 19.5\%$ for the largest one (100 cells), with the particular situation of a marked proportional increase of the standard deviations as the number of cells augments. Specifically, the averaged calculations of E^P variate between 4.9 ± 0.52 and 19.5 ± 4.5, which means an increase of the standard deviations from 10.6% for the smallest sub-population to 23.1% for the largest one. A possible explanation of this fact is the increase of the variables (columns in the matrix of Table 4.2) when more cells are included into the sub-populations. Another explanation is the increase of stimuli that have to be classified, i.e. from nine stimuli in the case of velocities to 72 stimuli in the case of velocity transitions. These two aspects produce a reduction of the statistical information from each stimulus and consequently wider probability distributions.

Figure 4.3a shows also the improvements in the mean values of E^P that can be reached when the coding strategy $t_1\&t_2\&t_3$ was evaluated (black line). In this way, the results of correct estimation in function of the number of cells variates between $\sim 6.5\%$ for the smallest sub-population (5 cells) and $\sim 20.9\%$ for the largest one (100 cells); this means an improvement of $\sim 14\%$ in the classification. On the other hand, in the evaluation of both coding strategies t_1 and $t_1\&t_2\&t_3$ it is possible to distinguish a saturation in the mean values of the percentages of correct estimation when the sub-populations contained more than 40 cells. Nevertheless, this saturation is not so noticeable like the one observed for classification of velocities in Figure 4.2a. Moreover, it can be observed clearly that the standard deviation bars from the evaluation of both coding strategies, t_1 and $t_1\&t_2\&t_3$, are widely overlapped for all the sub-populations. However, this fact may be explained due to the reduction of the statistical information for classification of velocity transitions, which has been mentioned above.

Figure 4.3b presents the differences $(\Delta E^P(N))$ between the improvement reached when t_2 and t_3 were included together to t_1 for the classification (gray line) in contrast with the improvement including only t_2 (black line). These differences were also calculated by Equations 4.5; as can be noticed, there are not evident increases in the classification of velocity transitions when the third spike is included in the analysis. In both cases, inclusion of $t_2\&t_3$ to t_1, as

well as inclusion of only t_2, provided an enhancement of classification between ~ 1.4 and $\sim 3.2\%$, depending of the number of cells (N). A possible explanation of this behavior is that in this study the estimation of the temporal information of the third spikes was included as an indirect way for estimation of spike count; according to the work published by Winzenborg et al. (2010), most of the information of velocities is encoded by spike count, whereas the information of velocity transitions is best encoded via latencies. In the case of the work presented in this thesis, the third spikes (t_3^c) could be included information that is somehow uncorrelated with the latencies (t_1^c) when one wants to decode velocity transitions instead of velocities. Nonetheless, the second spikes (t_2^c) were also included in the classification procedure as indirect way to estimate spike count, whose combination with latencies improved the classification of velocity transitions [3]. Additionally, it can be observed in Figure 4.3b an apparent peak of improvement when the sub-populations contain about 40 cells, specially by evaluation of $t_1\&t_2\&t_3$. Like observed in Figure 4.2b, both curves descend systematically as the number of cells (N) increases. However, a possible reason of this behavior is possibly the large artificial estimations of 150 ms assigned to t_2^c and t_3^c, as presented in the analysis of Figure 4.3b.

The analysis of misclassification is performed separately from velocities before the triggers (Figures 4.3c and 4.3e) and after the triggers (Figures 4.3d and 4.3f). In Figure 4.3c it is observed that estimation error of speeds in the velocities before the triggers did not decreased considerably as the size of the sub-populations (N) increased, such as had be observed in Figure 4.3c for classification of velocities. Only minor reductions of the absolute mean error (E^S) can be noticed when the reconstruction is performed from sub-populations with less than 30 cells. In addition, there is no reductions of the absolute error by evaluation of $t_1\&t_2\&t_3$ in relation to the the evaluation of only t_1 either. Nonetheless, the values of E^S keep substantially low (between ~ 0.3 to ~ 0.5) compared with the chance level indicated by the dotted line, regardless the coding strategy evaluated. In contrast, Figure 4.3d shows that the speeds are likely to be wrong classified when the sub-populations contained less than 25

---

[3]In fact, from the study presented by Winzenborg et al. (2010), classification of velocity transitions by evaluation of only latency is better than by evaluation of latency combined with spike count
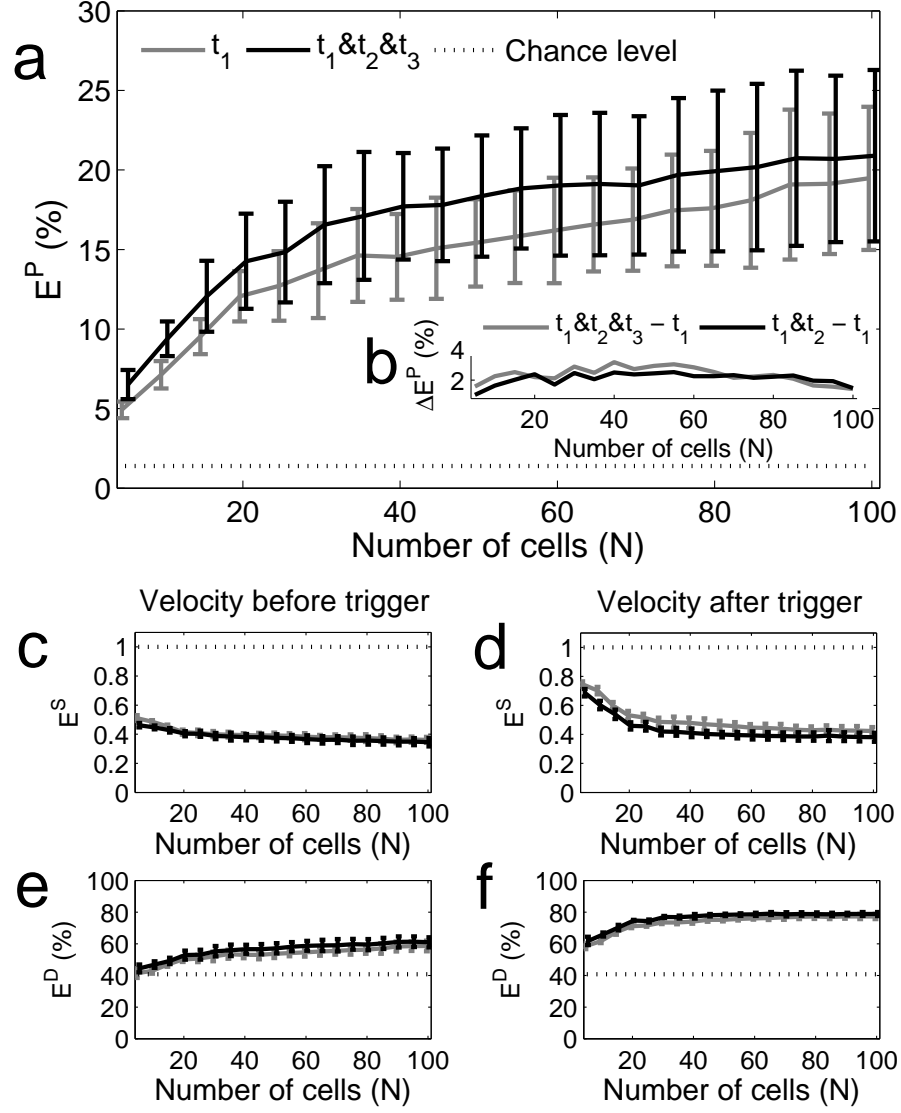
Figure 4.3: Results of performance measures for classification of velocity transitions. a) Percentages of correct estimation (E^P). b) Differences of classification between inclusion of t_2 and t_3 to t_1 and inclusion of only t_2 (see text). c) and d) Absolute mean errors (E^S) from the classification of speeds in the velocities before and after trigger respectively. e) and f) Percentages of correct estimation in the classification of directions (E^D) for the velocities before and after trigger respectively.

cells; for the smallest sub-populations (5 cells), the mean values of E^S were ~ 0.51 by evaluation of t_1 and ~ 0.46 by evaluation of $t_1 \& t_2 \& t_3$. However, when the number of cells in the sub-populations got larger than 25 cells, the mean values of E^S stabilized systematically until the largest sub-population (100 cells), getting a value of ~ 0.36 by evaluation of t_1 and ~ 0.34 by evaluation of $t_1 \& t_2 \& t_3$. The analysis of Figure 4.3d shows also that the mean values of the curves are noticeably separated for sub-populations constructed with less than 65 cells, which suggests a slight improvement in the detection of speeds when t_2 and t_3 are combined with t_1. For instance, by evaluation of $t_1 \& t_2 \& t_3$ and using a sub-population with intermediate size (50 cells), the averaged value of E^S is 0.37 ± 0.02 for velocities before the trigger and 0.39 ± 0.1 for velocities after the trigger.

Figure 4.3e shows the percentages of correct estimations (E^D) for velocities before the triggers. From the observation of this Figure, it is evident that the smallest sub-populations exceeded hardly the chance level (40.74%). For instance, in the sub-population of 5 cells the mean value of E^D by evaluation of t_1 is $\sim 41.4\%$. Nevertheless, the performance in the prediction of motion directions shows a gradual enhancement as the number of cells augments, reaching a mean value of $\sim 52\%$ for a sub-population with 30 cells. From this point, the contribution per cell included gets less significant, so the performance in the prediction of directions reaches a maximum of $\sim 58.6\%$ for the largest sub-population (100 cells). The inclusion t_2 and t_3 to the analysis improves slightly the classification (between ~ 2.2 and $\sim 4.1\%$ depending on the number of cells in the sub-population).

The tendencies observed in Figure 4.3e can be likewise observed in the prediction of directions after the triggers shown in Figure 4.3f, excepting that in this last case the performance is better. For instance, by evaluation of t_1 and from the smallest sub-population (5 cells) the mean value of E^D reaches $\sim 58.4\%$, whereas for the largest one the mean value is $\sim 61.8\%$. That means an improvement of $\sim 18\%$ for classification of motion directions after the triggers in comparison to the classification before the triggers. Furthermore, inclusion of t_2 and t_3 does not entail an improvement in this performance.

4.5 Selected cells vs. random cells

In Section 3.9 it was accomplished a procedure to confirm the hypothesis that ganglion cells selected with systematic methods allow to obtain better classification performances of motion in comparison with randomly selected cells. This analysis was based on the evaluation of the coding strategy $t_1 \& t_2$ utilizing sub-populations constructed with the top-10 cells from the rankings of each evaluated method (visual inspection of rasters plots, reliability, directionality, discriminability and transmitted information). In addition, their classification performances were compared with the obtained using 100 sub-populations constructed each with 10 selected randomly cells. In this way, it was observed that cells selected by evaluation of their discriminability features allow to obtain the best classification performance and were thus selected to reconstruct the stimuli, such as has been described in Sections 4.2, 4.4.1 and 4.4.2.

In the present Section, it is evaluated this hypothesis in sub-populations constructed with different number of cells (N). Figure 4.4 shows the differences between the percentages of correct classification (E^P) for velocities and velocity transitions using the sub-populations selected by evaluation of their discriminability, in comparison with sub-populations constructed with cells randomly selected [4]. Initially, Figure 4.4a shows the values of E^P for reconstruction of velocities (black solid line) in the same form as indicated in Figure 4.2a. Likewise, the classification using sub-populations with randomly selected cells are depicted with light gray solid curves. These curves have been overlapped trying to give a fair idea about the reconstruction efficiency from their respective sub-populations. According to the analysis of Figure 4.2a, there is a predominant benefit caused by the selection of cells when the reconstruction is accomplished using small sub-populations. Specifically, the overlap between the black curve (selected cells) and the light gray curve (random cells) is not very marked when the sub-populations were constructed with less than 40 cells. In addition, since the selection of cells to construct the random sub-populations was repeated 100 times, the averaged mean values $\widetilde{E^P}(N)$ for each

---

[4]In this case, the location of these points over the curves were also slightly shifted to avoid possible horizontal overlapping of the standard deviation bars between them. This was intended for a better visualization of the results

of these sub-populations were calculated as follow:

$$\widehat{E^P}(N) = \frac{1}{100}\sum_{i=1}^{100}\overline{\widetilde{E_i^P}(N)}, \qquad (4.7)$$

where $\overline{\widetilde{E_i^P}(N)}$ represents the mean value of the percentages of correct estimation computed in an iteration i from a sub-population with N random ganglion cells. The values of $\widehat{E^P}(N)$ are depicted by the black dashed curve in Figure 4.4a. In addition, it is possible to obtain one idea about the benefit of the selection of cells by the difference between the classification with systematically selected cells and randomly selected ones [5]. This difference was calculated as follow:

$$\Delta E^P(N) = \overline{E^P(N)} - \widehat{E^P}(N), \qquad (4.8)$$

where $\overline{E^P(N)}$ indicates the mean values computed from the percentages of correct estimation in each sub-population with N systematically selected cells [6]. The values of $\Delta E^P(N)$ are thus represented by the curve in the Figure 4.4b. As expected, the improvement in the performance of estimation is more evident when the velocities were estimated using small sub-populations; it can be noticed a peak of more than 9% in the values of $\Delta E^P(N)$ when the comparison is made for sub-populations of 20 cells and the curve descends gradually as the number of cells (N) increases. Figures 4.4c and 4.4d show the same analysis for reconstruction of velocity transitions. From the observation of Figure 4.4c it can be noticed that the standard deviation bars of the black curve (selected cells) are more overlapped with the ones of the light gray curve (random cells), which indicates that the benefit of the selection of cells in the reconstruction of velocity transitions is minor. The curve in Figure 4.4d represents the difference computed from Equation 4.8. In this case, it can be also noticed a peak for sub-populations of 20 cells, indicating a peak of a bit more than 5% in the values of $\Delta E^P(N)$.

For a better understanding of these comparisons, a t-test was accom-

---

[5]Systematically selected cells are those that result from the calculation of discriminability.

[6]Notice that the values of $\Delta E^P(N)$ calculated by Equation 4.8 is different from the ones computed by means of Equation 4.5.
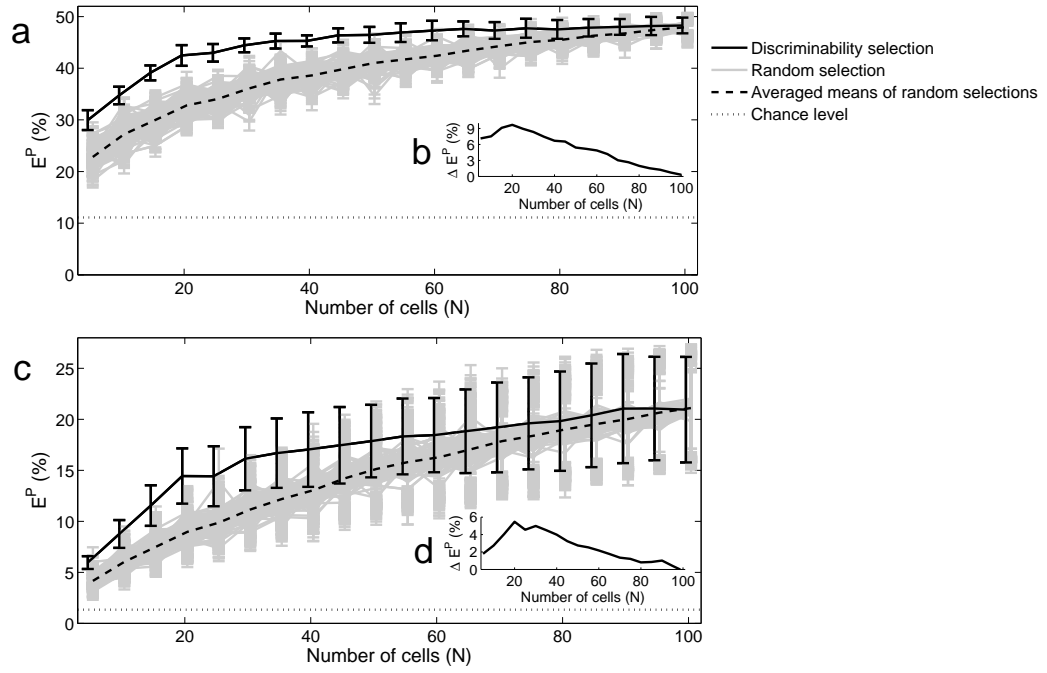
Figure 4.4: Comparison of the classification efficiency between sub-populations constructed with cells selected by discriminability and sub-populations with random selected cells. Figures a and b show the results for reconstruction of velocities, whereas Figures c and d are the results of comparison for reconstruction of velocity transitions (see text). The coding strategy evaluated was $t_1 \& t_2$.

plished by means of the function `ttest2` of Matlab® Statistics Toolbox. Basically, the p-values were computed for each number of cells N between the sub-populations with systematically selected cells and each of the 100 sub-populations constructed with random cells. In this way, the function `ttest2` performs a t-test of the null hypothesis that data in vectors x and y are independent random samples from normal distributions with equal means and equal but unknown variances, against the alternative that the means are not equal. In this case, x is the vector of computed values of E^P from the sub-population with systematically selected cells and y represents the vectors of the calculations of E^P using one of the 100 sub-populations with random cells. The null hypothesis was rejected at the 5% significance level and the p-values were computed by `ttest2` as the probability, under the null hypothesis, of observing a value as extreme or more extreme of the test statistic calculated as follow:

$$t(N) = \frac{\overline{x(N)} - \overline{y(N)}}{\sqrt{\frac{\sigma^2_{x(N)}}{n_{x(N)}} + \frac{\sigma^2_{y(N)}}{n_{y(N)}}}} \tag{4.9}$$

where $\overline{x(N)}$ and $\overline{y(N)}$ are the vectors means, $\sigma^2_{x(N)}$ and $\sigma^2_{y(N)}$ are the sample standard deviations and $n_{x(N)}$ and $n_{y(N)}$ are the vectors sizes. Figure 4.5 presents the averaged p-values computed between the pairs of vectors denoted by x and y. The means and standard deviations were calculated due to the 100 iterations of t-test for each number of cells (N). In the case of velocities, values $p<0.005$ were obtained for sub-populations that contained between 5 and 60 cells. In contrast, values $p<0.005$ were obtained for velocity transitions only from the sub-populations with 15 and 20 cells. This fact confirms that the profit of selecting cells in major for prediction of velocities using sub-populations of small and medium size than for prediction of velocity transitions.

4.6 Optimal size of sub-population

The results presented in Sections 4.4.1, 4.4.2 and 4.5 have allowed to observe that the percentages of correct classification (E^P) augmented as the number of cells (N) of the sub-populations increased. Nevertheless, there are some values
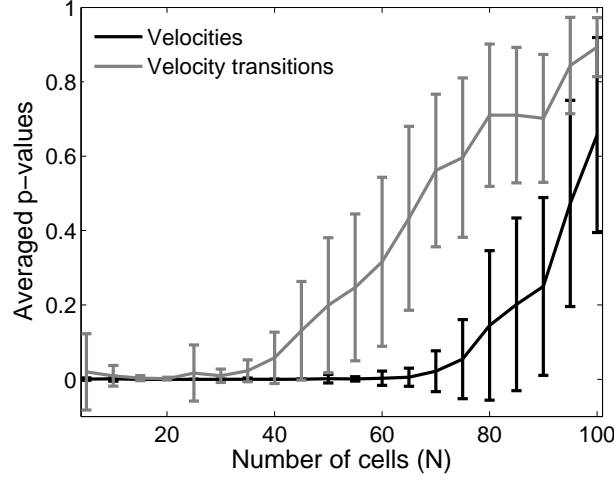
Figure 4.5: Mean of the p-values obtained by t-test performances between the percentages of correct estimations from sub-populations with systematically selected cells and sub-populations with random cells.

of N from which the contribution of the cells included to enhance the results of classification is minor. This situation is clearly evident due to the saturation or plateau in reconstruction of velocities (Figures 4.2a and 4.4a) and in lesser extent in reconstruction of velocity transitions (Figures 4.3a and 4.4c). In this step, it is defined an optimal number of cells (N) for reconstruction of motion relative to the maximum contribution given by the largest sub-populations. To give a better idea about it, let $E^P(N_{\max})$ be the classification performance obtained from the largest number of cells (in this case, $N_{\max}=100$) [7], the contribution ($K(N)$) per cells included in the sub-populations to enhance the classification performances was calculated relative to $E^P(N_{\max})$ as follow:

$$K(N) = E^P(N_{\max}) - E^P(N) \tag{4.10}$$

where $E^P(N)$ is the percentages of correct classification in function of N calculates from Equation 3.19. Subsequently, it was defined a level of $K(N)$

---

[7]The values of E^P were obtained by evaluation of the coding strategy $t_1\&t_2\&t_3$ and using the sub-populations constructed with systematically selected cells.

to establish the point in which the contribution per cells included in the sub-populations starts to minimize. The procedure to fix this level is somehow subjective, since it may depend on the own considerations of the observer. To clarify this procedure, the level has been established as 5% of the maximum contribution given by $K(N)$, which is represented by the horizontal dotted lines in the plots of Figure 4.6 [8]. The vertical dotted lines match the level of 5% with the optimal number of cells (N) that would be relative enough to obtain good performances of reconstructions, which are indicated by the arrows inside the plots (~ 55 cells for velocities and ~ 84 cells for velocity transitions). Contributions of cells included in the sub-populations beyond the number indicated by the arrows do not entail a significative improvement of the classifications.
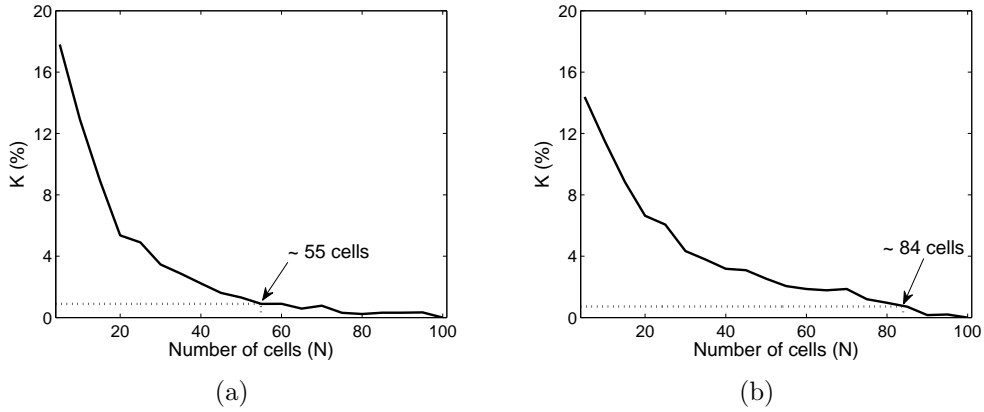

Figure 4.6: Contribution $(K(N))$ per cells included in each sub-population. The calculations were accomplished relative to the classification performance reached for $N_{\text{max}}=100$. (a) $K(N)$ for velocities; (b) $K(N)$ for velocity transitions.

4.7 Dependence of the trigger

The accuracy in the estimation of t_1^c, t_2^c and t_3^c is highly influenced by the triggers (e_t) detected in the procedure briefly described in Section 2.4. Hence,

---

[8]Naturally, it could be likewise valid to establish this level in ranges close to 5%.

the classification efficiency of velocities and velocity transitions may depend highly on the performance of the algorithm to detect the triggers that have been applied in this work. The task to obtain an algorithm for detection of transitions without errors is very difficult. On the one hand, different parameters of the algorithm had to be adapted to find its best performance, which was established to minimize the detection of false triggers (Winzenborg et al., 2010). On the other hand, there are transitions of stimuli very hard to detect, specifically those ones whose speeds do not change considerably and whose directions are the same before and after the stimulus transition. In the present work, it was introduced a procedure to modify the time points of the triggers e_t and evaluate the classification efficiency for velocities and velocity transitions.

In this procedure two kinds of variations were included. The first one consisted of inclusion of a time delay after every trigger detected by the algorithm. The times of these delays were 10, 20 and 30 ms, in such a way that all the trials in the data set were homogeneously delayed including each of these time values. The second variation was accomplished by random delays obtained by means of Gaussian noise with standard deviation values of 2, 4, 6, 8 and 10 ms. Subsequently, the temporal information of t_1^c, t_2^c and t_3^c (Section 4.1) was estimated again and the stimuli (velocities and velocity transitions) were reconstructed as described in Sections 4.4.1 and 4.4.2 by evaluation of the coding strategy $t_1 \& t_2 \& t_3$. To determine how much the results of classification were improved or diminished due to these modifications in the triggers (e_t), an index ID (improvement-diminishing) was computed as follow:

$$ID_{E^P}(N) = \widetilde{E}^P_{t_1 \& t_2 \& t_3}(N) - E^P_{t_1 \& t_2 \& t_3}(N) \tag{4.11}$$

where $\widetilde{E}^P_{t_1 \& t_2 \& t_3}(N)$ and $E^P_{t_1 \& t_2 \& t_3}(N)$ represent the percentages of correct estimations with and without delayed triggers respectively. In similar form, the indexes to determine how improved or diminished were the estimations of speeds and directions of the motions are indicated as follow:

$$ID_{E^S}(N) = \widetilde{E}^S_{t_1 \& t_2 \& t_3}(N) - E^S_{t_1 \& t_2 \& t_3}(N) \tag{4.12}$$

$$ID_{E^D}(N) = \widetilde{E}^D_{t_1 \& t_2 \& t_3}(N) - E^D_{t_1 \& t_2 \& t_3}(N) \tag{4.13}$$

Plots in Figure 4.7 show the results of these calculations for classification of velocities. As can be observed, the estimation of velocities enhanced as the time of delay increased. This fact can be explained because the delay times included after the triggers e_t may entail the estimation of the time points given by t_1^c, t_2^c and t_3^c within time windows of trials that contain a more stationary response.
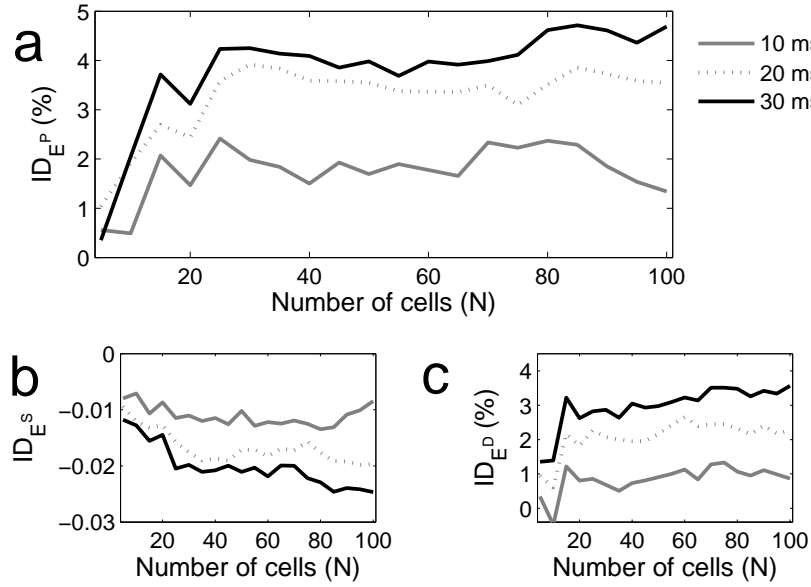

Figure 4.7: ID indexes computed with homogeneous delaying in the classification of velocities for a) percentages of correct estimation (E^P), b) absolute mean errors (E^S) and c) percentages of correctly estimated directions (E^D). The legend indicates the notation of the results according to each of the three time delays introduced.

The improvement in the estimation of velocities augmented as the time delay increased, reaching for instance enhancements between 4 and 5% when the delay time is 30 ms (Figure 4.7a), as well as improvements between 3 and 4% in the estimation of directions (Figure 4.7b) and reductions in the absolute errors (Figure 4.7c). These improvements have a slight tendency to be more evident as the number of cells (N) in the sub-populations increased, specially from Figures 4.7b and 4.7c. Likewise, the differences between estimation of velocities with time delays of 20 and 30 ms are not so far away from each other.

This fact allows to suppose that improvements caused by the inclusion of these time delays would not be very significant whether the estimations of t_1^c, t_2^c and t_3^c were performed beyond 20 or 30 ms after the triggers e_t. Furthermore, inclusion of time delays longer than 30 ms would entail longer times required by the brain to process the encoded information from the retina, which would not be feasible from a biological point of view.

Figure 4.8 shows the calculations of the indexes $ID_{E^P}(N)$, $ID_{E^S}(N)$ and $ID_{E^D}(N)$ when the triggers e_t were randomly delayed. As expected, the classification performance diminished as the standard deviation of the Gaussian noise augmented. From the observation of the Figure 4.8a it can be noticed a slight reduction until $\sim 1\%$ when the standard deviation value of the Gaussian noise did not exceed 6 ms. Reductions until $\sim 2.4\%$ can be found whether the Gaussian noise is applied with a standard deviation of 10 ms. Naturally, this observation is consistent with the enhancement of the absolute errors (Figure 4.8b) and decrease of the percentages of correctly estimated directions (Figure 4.8b) as the standard deviation values increased. In this last case, the prediction of direction was diminished in $\sim 1\%$ with the maximal standard deviation (10 ms). Despite the obervations, the random time delays employed to modify the position of the triggers did not entail a strong reduction in the performance for classification of velocities; the largest reduction in the mean values of E^P ($\sim 2.4\%$) is small whether it is compared with the maximum mean values of E^P obtained without delayed triggers by evaluation of the coding strategy $t_1\%t_2\%t_3$ (between~ 31 and $\sim 49\%$ observed from Figure 4.3a).

In the case of velocity transitions, the homogeneous delaying produced also a slight reduction in the classification performance, which variates between ~ 0.5 to $\sim 2\%$ when the triggers were delayed in 30 ms (Figure 4.9a); reductions caused by time delays of 10 and 20 ms were not quite different from those when the time delay is 30 ms. It can be observed from Figures 4.9b and 4.9d that the classification performance of velocity transitions was diminished because the delaying of the triggers entailed a reduction in the estimation of velocities before the transition of stimuli; the absolute error values augmented (Figure 4.9b) and the percentages of correctly estimated directions reduced to $\sim 2\%$ when the time delay was 30 ms. In contrast, the velocities after the transitions were better classified (Figures 4.9c and 4.9e), although it is clear
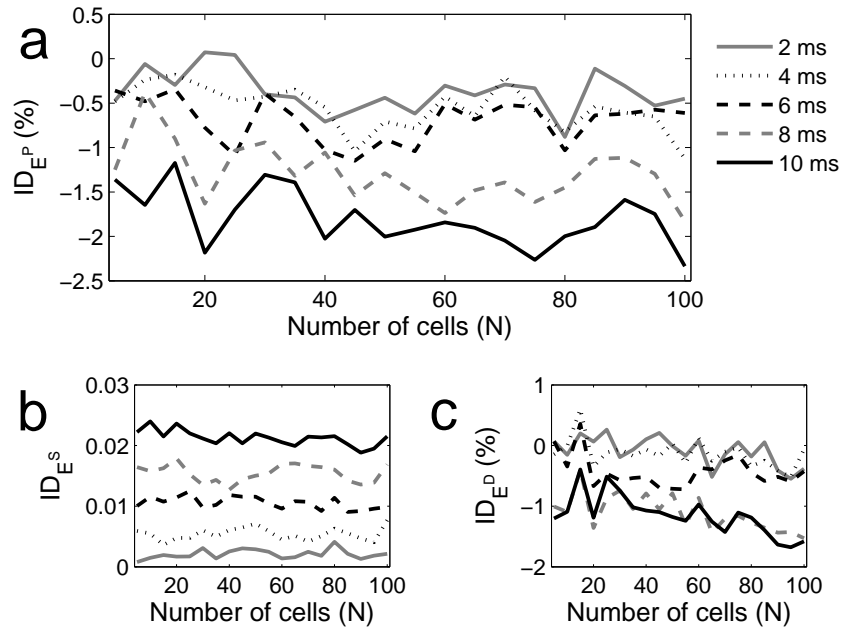
Figure 4.8: ID indexes computed with random delaying in the classification of velocities for a) percentages of correct estimation (E^P), b) absolute errors (E^S) and c) percentages of correctly estimated directions (E^D). The legend indicates the notation of the results according to each of the standard deviation values.

that this fact is caused by the tendency to estimate the coding strategies in more stationary periods of the response after the triggers, such as observed in the plots of Figure 4.7. It is probably that information about the stimuli before the transitions, which are present during few milliseconds after the detected triggers (e_t), disappeared when these ones were delayed. The reduction in the classification performance is not considered significant either. In this case, the largest reduction in the mean values of E^P ($\sim 2\%$) is small compared with the maximum mean values of E^P obtained without delayed triggers, i.e. $\sim 20.89\%$ from the largest sub-population (100 cells) by evaluation of the coding strategy $t_1\%t_2\%t_3$ (Figure 4.3a).

The plots in Figure 4.10 show the calculations of the indexes $ID_{E^P}(N)$, $ID_{E^S}(N)$ and $ID_{E^D}(N)$ when the triggers e_t were randomly delayed. It can be noticed that the deterioration of the reconstruction has a tendency to get worst as the number of cells in the sub-populations increased, specially when the standard deviation of the Gaussian noise applied had values of 6, 8 and 10 ms. In this last case, the mean values of E^P were diminished to $\sim 3.5\%$ by reconstruction from the largest sub-population (100 cells). In comparison to the maximum deterioration caused by homogeneous delaying observed in Figure 4.9a (~ 0.5 - $\sim 2\%$), it could be suggested that the larger deterioration caused by random delaying (~ 0.5 - $\sim 3.5\%$) is consequence of the additional misclassification of velocities after the trigger (Figures 4.9c and 4.9e).
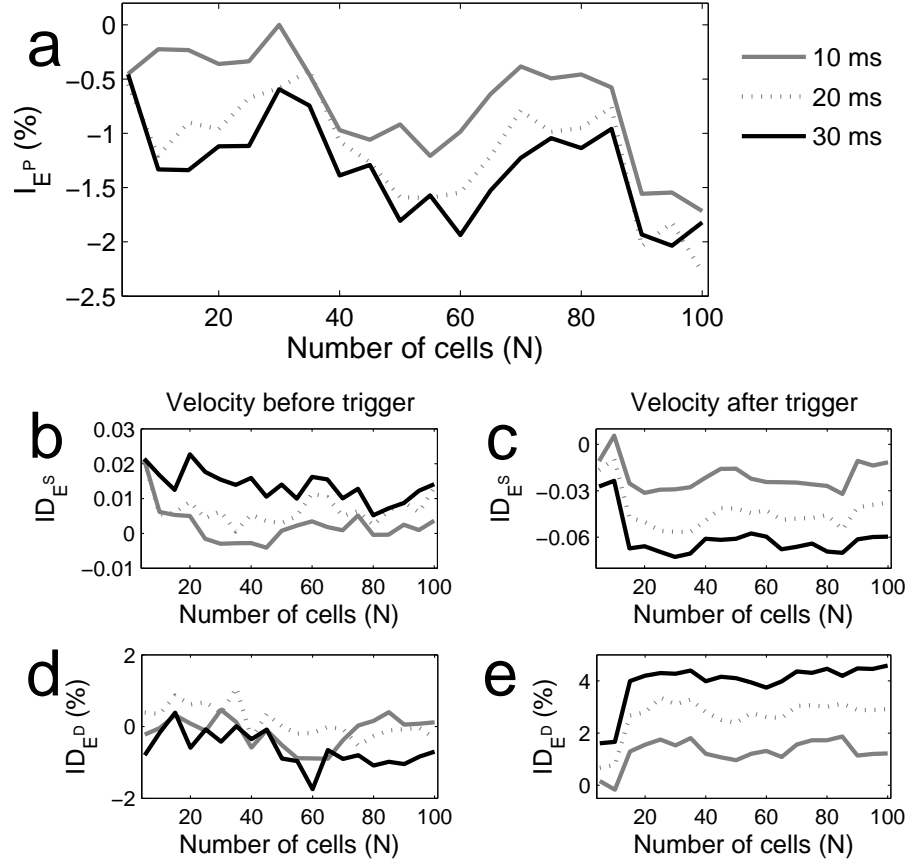
Figure 4.9: ID indexes computed with homogeneous delaying in the classification of velocity transitions for a) percentages of correct estimation (E^P); b) absolute mean errors (E^S) and d) percentages of correctly estimated directions (E^D) before the delayed triggers; c) absolute mean errors (E^S) and e) percentages of correctly estimated directions (E^D) after the delayed triggers. The legend indicates the notation of the results according to each of the three time delays introduced.

Figure 4.10: ID indexes computed with random delaying in the classification of velocity transitions for a) percentages of correct estimation (E^P); b) absolute mean errors (E^S) and d) percentages of correctly estimated directions (E^D) before the delayed triggers; c) absolute mean errors (E^S) and e) percentages of correctly estimated directions (E^D) after the delayed triggers. The legend indicates the notation of the results according to each of the standard deviation values.
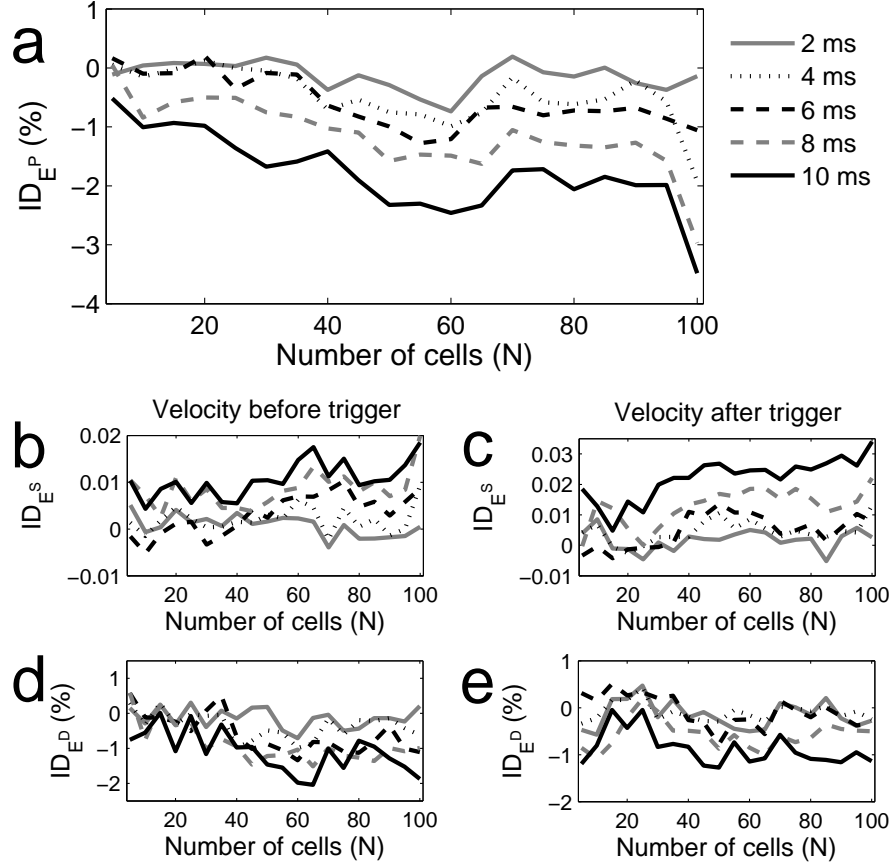
Chapter 5

Summary and conclusions

In this thesis, it has been developed a method oriented to reconstruct visual motion stimuli (velocities and velocity transitions) in a fast and efficient way, i.e. by decoding of information in a short time window (150 ms) and using a minimum possible number of cells. The following Sections summarize the analysis accomplished in this work with the corresponding discussions and conclusions.

5.1   Selection of cells

Five methods for selection of cells have been presented in this thesis: a) visual inspection of raster plots, b) reliability, c) directionality, d) discriminability and e) transmitted information by calculation of Shannon's mutual information. Whereas the first method involves the subjectivity inherent in one observer to describe the raster plots, the other four methods analyze the responsivity of individual cells based on different properties computed from their firing patterns. Naturally, it can be suggested that the higher responsivity of a cell the higher capacity that this has to detect changes of stimuli, even when these changes are minor. It is important to remind that each of the properties above mentioned were quantified and ranked from the highest to the lowest value. In this manner, a hierarchical ranking of cells was obtained for each of these properties according to their respective ranked values.

Initially, it was assumed that the responsivity of the ganglion cells may be

directly estimated from its firing rate; the direction selective cells modulate their responses in function of the speed (Figure 3.1) and direction (Figure 3.5) of the applied stimulus velocity. In such a way, the calculation of directionality was intended to assess the asymmetry of the tuning curves based on variations of their firing rates in response to every stimulus. However, the directionality values from each cell shown to be anti-correlated with the firing rate, which determined via estimation of spike count (Figure 3.6(b)). This anticorrelation was probably caused by the high variability of the responses, which may entail a reduction in the responsivity of the cells. For this reason, the measure of discriminability was introduced to quantify the responsivity of every cell taking into account such variabilities in their responses. Specifically, the calculation of discriminability was based on the standard deviation of the spike count values from each cell in response to one of the applied stimulus velocities. In this case, it has been observed a noticeable positive correlation between discriminability and firing rate (Figure 3.7(b)). Likewise, it was suggested that responsivity could be evaluated from the timing of their spikes. This property was quantified via reliability measure, assuming that responsivity would be higher in cells with reliable firing pattern across trials in response to a stimulus velocity. Since this measure is based on spike timing instead of firing rate, it would be obvious for reliability to be anti-correlated with spike count (Figure 3.4(b)). However, such anti-correlation could indicate that the measure of spike timing reliability prefers cells that respond very weakly to stimulus velocities.

In order to evaluate of the methods for selection of cells, the reconstruction of velocities and velocity transitions was accomplished (see Sections 3.7 to 3.9). Specifically, small sub-populations of 10 cells each were constructed using the top ten cells from each of the hierarchical rankings. Subsequently, a coding strategy based on the temporal information of the first two spikes was defined, whose estimation was made within the 150 ms following the response triggers (defined as time points in which substantial changes of the population firing rate occur). The reconstruction within this short time window was imposed on this analysis because behavioral response is typically observed to occur not later. The spike times of individual cells were estimated via single-trial and then the decoding was performed by means of a classifier based on linear dis-

criminant analysis. In this task, the results of classification were compared with sub-populations made with randomly selected cells. It was observed that the sub-populations constructed with cells selected by evaluation of discriminability allowed to obtain the better classification efficiency (Figure 3.11). In any way, it has been somehow surprise that spike count discriminability turned out to be more efficient than a reliability measure for spike timing.

5.2 Evaluation of fast coding strategies

The reconstruction of velocities and velocity transitions was accomplished in similar form as in the selection of cells. However, in this step a wider analysis of the fast coding strategies was included. These coding strategies were basically defined as follow: a) latency or first spike timing (t_1), latency combined with second spike timing (t_1&t_2) and latency combined with second and third spikes timings (t_1&t_2&t_3). Estimation of t_2 and t_3 entailed to include two interspike intervals into the analysis, i.e. t_2 - t_1 and t_3 - t_2. Since latencies in this study have shown to be inversely proportional to firing rates, t_1 alone can be considered as the simplest way to estimate spike count. Therefore, it was established the hypothesis that including the interspike intervals could improve the reconstruction of the motion stimuli, having into account that estimation of t_2 and t_3 have been considered as indirect forms to estimate firing rate. Another consideration is that the firing frequency of the cells have shown to be very low in 150 ms, for which simple spike counts are too coarse to resolve complex stimuli; the possibility to reconstruct important stimuli features, via directly estimated spike count, is relatively limited.

It has been observed from results in Sections 4.2 and 4.4 that latencies (represented by t_1) contain most of the encoded information for reconstruction of motion stimuli. As expected, the coding strategies represented by combinations of t_1 with t_2 and t_3 led to moderate improvements in the reconstructions, probably because the estimate provided by the latency is already quite accurate. Furthermore, a particular situation observed in these results is the difficulty to decode directions correctly using sub-populations made with less that 30 cells. Probably, few selective to direction cells were included in the highest places of the discriminability ranking. In any way, the whole database

acquired from the experiment contains a reduced number of this kind of cells. Likewise, this analysis shows that reconstructions are significative better in sub-populations with systematically selected cells than in sub-populations constructed with randomly selected cells [1]. This fact is specially noticeable when the reconstructions were accomplished using sub-populations constructed with less than 45 or 50 cells (Figure 5.1a).

In addition, inclusion of t_2 and t_3 as indirect ways to estimate spike count has shown to be complement of the encoded information supplied by only t_1. Levels of classification reached with large sub-populations evaluating only t_1 can be also obtained without loss of efficiency using reduced sub-populations and combining t_1 with t_2 and t_3 (Figure 5.1b). The reason is that building sub-populations by systematically selected cells with highest discriminability rapidly accumulates the major share of efficiency, whereas the remaining bulk of cells does not contribute much more. To strive for small sub-populations is, of course, motivated by an economic rationale. From the plots of Figure 5.1 it can be observed that the maximum classification efficiency is actually achieved when all the cell were collected in the largest sub-population. If there were no computational or metabolic cost per cell added the recommendation would, indeed, be to perform the reconstruction with all accessible cells, the more the better.

The discriminant analysis used for reconstruction in this study has produced similar results in comparative studies with other reconstruction methods, e.g. Bayesian classifier (Winzenborg et al., 2010). Therefore, it is considered that the conclusions drawn here are not reconstruction method specific. Additionally, there is no evidence that use of different classification methods lead to variations in the classification efficiency (Warland et al., 1997; Frechette et al., 2005).

---

[1]It is worth remembering that systematically selected cells are those that result from the calculation of discriminability
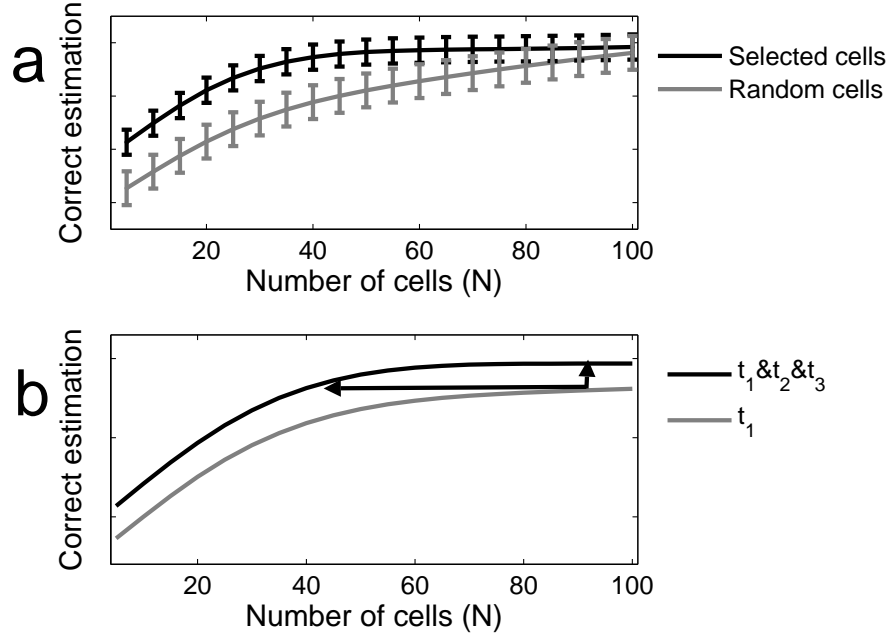
Figure 5.1: Reconstruction efficiency measured via percentages of correct estimations (E^P). The curves displayed in both panels are smoothed versions of related curves seen in panels a of Figures 4.2 and 4.3. Since this figure should only support the argumentation of the discussions, the tick marks have been omitted along the ordinates. a) Illustration of the efficiency gain when changing from randomly compiled sub-populations to ensembles that preferentially combine ganglion cells with high discriminability. The well separated error bars indicate that for small sub-populations the difference is indeed statistically significant. b) Efficiency gain when supplementing the latency t_1 by spike times t_2 and t_3. Even though the gain is moderate (vertical arrow) the flat profile makes clear that the efficiency of the latency code t_1 for a large population can be maintained for a much smaller sub-population when supplementing spike times t_2 and t_3 (horizontal arrow).

5.3 Optimal number of cells for reconstruction of the stimuli

Finally, an optimal number of cells for reconstruction of the motion stimuli was defined by means of a partially subjective method. In this case, optimal

number of cells means a sub-population size from which inclusion of more cells does not allow a substantial improvement of the classification efficiency. The specification of a minimum number of cells, sufficient to reach good reconstruction performances, is physiologically motivated due to the cost that may imply the inclusion of more cells into the sub-populations. The analysis shown in Section 4.6 stated a break point from the curves E^P vs. N of 55 cells for classification of velocities and 84 cells for velocity transitions (Figure 4.6). These break points were estimated relative to the maximum contribution, i.e. from the classification efficiency reached using the largest sub-populations. Nevertheless, other methods lead to similar results. For instance, by calculation of the smallest slope when it is considered the contribution per included cell $\partial E^P/\partial N$.

Bibliography

Adrian, E., 1926. The impulses produced by sensory nerve endings: Part i. J. Physiol. (London) 61, 49–72.

Ammermueller, J., Muller, J., Kolb, H., 1995. The organization of the turtle inner retina. ii. analysis of color-coded and directionally selective cells. The Journal of Comparative Neurology 358, 35–62.

Amthor, F., Tootle, J., Gawne, T., 2005. Retinal ganglion cell coding in simulated active vision. Visual Neuroscience 22, 789–806.

Ariel, M., Adolph, A., 1985. Neurotransmitter inputs to directionally sensitive turtle retinal ganglion cells. J Neurophysiol 54, 1123–1143.

Barlow, H., Levick, W., 1965. The mechanism of directionally selective units in rabbit's retina. J. Physiol. 178, 477–504.

Barnes, G., December 2008. Cognitive processes involved in smooth pursuit eye movements. Brain Cogn. 68 (3), 309–326.

Barnes, G., Donnelly, S., Eason, R., 1987. Predictive velocity estimation in the pursuit reflex response to pseudo-random and step displacement stimuli in man. J. Physiol. 389, 111–136.

Berry, M., Brivanlou, I., Jordan, T., Meister, M., March 1999. Anticipation ofmoving stimuli by theretina. Nature 398, 334–338.

Berry, M. J., Warland, D. K., Meister, M., 1997. The structure and precision of retinal spike trains. Proc. Natl. Acad. Sci. USA 94, 5411–5416.

Bialek, W., Rieke, F., de Ruyter van Steveninck, R., Warland, D., 1991. Reading a neural code. Science 252, 1854–1857.

Bonnasse-Gahot, L., Nadal, J., 2008. Neural coding of categories: information efficiency and optimal population codes. J Comput Neurosci 25, 169–187.

Borst, A., Theunissen, F., 1999. Information theory and neural coding. Nat. Neurosci. 11, 947–957.

Bowling, D., 1980. Light responses of ganglion cells in the retina of the turtle. J Physiol 299, 173–196.

Brivanlou, I., Warland, D., Meister, M., March 1998. Mechanisms of concerted firing among retinal ganglion cells. Neuron 20, 527–53.

Brunel, N., Nadal, J., 1998. Mutual information, fisher information, and population coding. Neural Computation 10, 1731–1757.

Chichilnisky, E., Kalmar, R., July 2003. Temporal resolution of ensemble visual motion signals in primate retina. The Journal of Neuroscience 23 (17), 6681–6689.

Dayan, P., Abbott, L., 2001. Theoretical Neuroscience: Computational and Mathematical Modeling of Neural Systems.

Delorme, A., Thorpe, S., 2001. Face identification using one spike per neuron: resistance to image degradation. Neural Networks 14, 795–803.

Demb, J., Haarsma, L., Freed, M., Sterling, P., November 1999. Functional circuitry of the retinal ganglion cell's nonlinear receptive field. The Journal of Neuroscience 19 (22), 9756–9767.

Demb, J., Sterling, K. Z. P., November 2001. Cellular basis for the response to second-order motion cues in y retinal ganglion cells. Neuron 32, 711–721.

Demb, J., Zaghloul, K., Haarsma, L., Sterling, P., October 2001. Bipolar cells contribute to nonlinear spatial summation in the brisk-transient (y) ganglion cell in mammalian retina. The Journal of Neuroscience 21 (19), 7447–7454.

Dunteman, G., 1984. Introduction to Multivariate Analysis. Sage Publications Inc., Beverly Hills, California: USA.

Elstrott, J., Anishchenko, A., Greschner, M., Sher, A., Litke, A., Chichilnisky, E., Feller, M., 2008. Direction selectivity in the retina is established independent of visual experience and cholinergic retinal waves. Neuron 58, 499–506.

Fernández, B., Ferrández, J., Ammermueller, J., Normann, R., 2000. Population coding in spike trains of simultaneously recorded retinal ganglion cells. Brain Research 887, 222–229.

Ferrández, J., Bolea, J., Ammermüller, J., Normann, R., Fernández, E., 1999. A neural network approach for the analysis of multineural recordings in retinal ganglion cells: Towards population encoding. In: IWANN 99, Lecture Notes on Computer Science. No. 1607. pp. 289–298.

Foffani, G., Morales-Botello, M., Aguilar, J., May 2009. Spike timing, spike count, and temporal information for the discrimination of tactile stimuli in the rat ventrobasal complex. The Journal of Neuroscience 29 (18), 5964–5973.

Foffani, G., Moxon, K., 2004. Psth-based classification of sensory stimuli using ensembles of single neurons. Journal of Neuroscience Methods 135, 107–120.

Frechette, E., Sher, A., Grivich, M., Petrusca, D., Litke, A., Chichilnisky, E., 2005. Fidelity of the ensemble code for visual motion in primate retina. J. Neurophysiol 94, 119–135.

Fried, S., Muench, T., Werblin, F., 2002. Mechanisms and circuitry underlying directional selectivity in the retina. Nature 420, 411–414.

Fried, S., Muench, T., Werblin, F., 2004. The circuitry underlying directional excitation and inhibition to ds cells. Invest. Ophthalmol. Vis. Sci 45, Assoc. Res. Vis. Ophthalmol. Meeting E-Abstr, 2266.

Gautrais, J., Thorpe, S., 1998. Rate coding versus temporal order coding: a theoretical approach. BioSystems 48, 57–65.

Gerstner, W., Kistler, W., 2002. Spiking Neuron Models: Single Neurons, Populations, Plasticity.

Ghose, G., Harrison, I., 2009. Temporal precision of neuronal information in a rapid perceptual judgment. J Neurophysiol 101, 1480–1493.

Gollisch, T., February 2009. Throwing a glance at the neural code: rapid information transmission in the visual system. HFSP Journal 3 (1), 36–46.

Gollisch, T., Meister, M., 2008. Rapid neural coding in the retina with relative spike latencies. Science 319, 1108–1111.

Green, D., Swet, J., 1966. Signal Detection Theory and Psychophysics. Wiley: New York.

Greschner, M., Bongard, M., Rujan, P., Ammermueller, J., 2002. Retinal ganglion cell synchronization by fixational eye movements improves feature estimation. Nature neuroscience 5, 341–347.

Greschner, M., Thiel, A., Kretzberg, J., Ammermueller, J., 2006. Complex spike-event pattern of transient on-off retinal ganglion cells. J. Neurophysiol 96, 1–12.

Gunninga, D., Adamsa, C., Cunninghama, W., Mathiesona, K., O'Sheaa, V., Smitha, K., Chichilnisky, E., Litkec, A., Rahmana, M., 2005. 30 μm spacing 519-electrode arrays for in vitro retinal studies. Nuclear Instruments and Methods in Physics Research A 546, 148–153.

Hu, E., Bloomfield, S., July 2003. Gap junctional coupling underlies the short-latency spike synchrony of retinal alpha ganglion cells. The Journal of Neuroscience 23 (17), 6768–6777.

Ilg, U., Thier, P., 2008. The neural basis of smooth pursuit eye movements in the rhesus monkey brain. Brain and Cognition 68 (3), 229–240.

Jones, K., Campbell, P., Normann, R., 1992. A glass/silicon composite intracortical electrode array. Annals of Biomedical Engineering 20, 423–437.

Kass, R., Ventura, V., Brown, E., 2005. Statistical issues in the analysis of neuronal data. J Neurophysiol 94, 8–25.

Kirchner, H., Thorpe, S., 2006. Ultra-rapid object detection with saccadic eye movements: Visual processing speed revisited. Vision Research 46, 1762–1776.

Kolb, H., 2003. How the retina works. Sigma Xi, The Scientific Research Society 91, 28–35.

Land, M., 1999. Motion and vision: why animals move their eyes. J Comp Physiol A 185, 341–352.

Lestienne, R., 2001. Spike timing, sychronization and information processing on the sensory side of the central nervous system. Prog. Neurobiol. 65, 545–591.

Levine, M., Jul-Aug 1997. An analysis of the cross-correlation between ganglion cells in the retina of goldfish. Visual Neurosci 14 (4), 731–739.

Lisberger, S., Morris, E., Tychsen, L., 1987. Visual motion processing and sensory-motor integration for smooth pursuit eye movements. Ann. Rev. Neurosci. 10, 97–129.

Lisberger, S., Westbrook, L., June 1985. Properties of visual inputs that initiate horizontal smooth pursuit eye movements in monkeys. The Journal of Neuroscience 5 (6), 1662–1673.

Manly, B., 2004. Multivariate Statistical Merhods: A primer. Chapman & Hall/CRC: USA.

Mastronarde, D., 1989. Correlated firing of retinal ganglion cells. Trends in Neurosciences 12 (2), 75–80.

Meister, M., Berry, M., 1999. The neural code of the retina. Neuron 22, 435––450.

Meister, M., Lagnado, L., Baylor, D., November 1995. Concerted signaling by retina ganglion cells. Science 270 (5239), 1207–1210.

Meister, M., Pine, J., Baylor, D., 1994. Multi-neuronal signals from the retina: acquisition and analysis. Journal of Neuroscience Methods 51, 95–106.

Murphy, G., Rieke, F., 2008. Signals and noise in an inhibitory interneuron diverge to control activity in nearby retinal ganglion cells. Nature Neuroscience 11 (3), 318–326.

Nicolelis, M., Ghazanfar, A., Stambaugh, C., Oliveira, L., Laubach, M., Chapin, J., Nelson, R., Kaas, J., November 1998. Simultaneous encoding of tactile information by three primate cortical areas. Nature neuroscience 1 (7), 621–630.

Nirenberg, S., Carcieri, S., Jacobs, A., Latham, P., 2001. Retinal ganglion cells act largely as independent encoders. Nature 411, 698–701.

Nirenberg, S., Latham, P., 1998. Population coding in the retina. Current Opinion in Neurobiology 8, 488–493.

Osborne, L., Bialek, W., Lisberger, S., March 2004. Time course of information about motion direction in visual area mt of macaque monkeys. The Journal of Neuroscience 24 (13), 3210–3222.

Perrett, D., Rolls, E., Caan, W., 1982. Visual neurones responsive to faces in the monkey temporal cortex. Exp Brain Res 47, 329–342.

Pillow, J., Shlens, J., Paninski, L., Sher, A., Litke, A., Chichilnisky, E., Simoncelli, E., August 2008. Spatio-temporal correlations and visual signalling in a complete neuronal population. Nature 454, 995–999.

Pola, J., Wyatt, H., 1992. Smooth pursuit: response characteristics, stimuli and mechanisms. In: Carpenter RHS, e. (Ed.), Eye movements, Vision and visual disfunction. Vol. 8. London: McMillan, pp. 138–156.

Reichardt, W., 1961. Autocorrelation, a principle for the evaluation of sensory information by the central nervous system. In: Rosenblith, W. (Ed.), Sensory Communication. Cambridge, MA: MIT Press, pp. 303–317.

Robinson, D., 1965. The mechanics of human smooth pursuit eye movement. J. Phy8iol. 180, 569–591.

Roska, B., Werblin, F., June 2003. Rapid global shifts in natural scenes block spiking in specific ganglion cell types. Nature Neuroscience 6 (6), 600–608.

Rossel, S., Corlija, J., Schuster, S., 2002. Predicting three-dimensional target motion: how archer fish determine where to catch their dislodged prey. The Journal of Experimental Biology 205, 3321–3326.

Schneidman, E., Berry, M., Segev, R., Bialek, W., 2006. Weak pairwise correlations imply strongly correlated network states in a neural population. Nature 440, 1007–1012.

Schreiber, S., Fellous, J., Whitmer, D., Tiesinga, P., Sejnowski, T., 2003. A new correlation-based measure of spike timing reliability. Neurocomputing 52–54, 925 —- 931.

Schwartz, G., Taylor, S., Fisher, C., Harris, R., Berry-II, M., September 2007. Synchronized firing among retinal ganglion cells signals motion reversal. Neuron 55, 958–969.

Segev, R., Goodhouse, J., Puchalla, J., Berry, M., 2004. Recording spikes from a large fraction of the ganglion cells in a retinal patch. Nature Neuroscience 7, 1155–1162.

Segev, R., Schneidman, E., Goodhouse, J., II, M. J. B., 2007. Role of eye movements in the retinal code for a size discrimination task. J. Neurophysiol 98, 1380–1391.

Shlens, J., Field, G., Gauthier, J., Grivich, M., Petrusca, D., Sher, A., Litke, A., Chichilnisky, E., 2006. The structure of multi-neuron firing patterns in primate retina. The Journal of Neuroscience 26 (32), 8254–8266.

Sommer, M., Wurtz, R., 2002. A pathway in primate brain for internal monitoring of movements. Science 296, 1480–1482.

Taketani, M., Baudry, M., 2006. Advances in Network Electrophysiology. Using Multi-Electrode Arrays. Springer.

Thiel, A., Greschner, M., Eurich, C., Ammermueller, J., Kretzberg, J., 2007. Contribution of individual retinal ganglion cell response to velocity and acceleration encoding. J Neurophysiol 98, 1–12.

Thorpe, S., 1990. Spike arrival times: A highly efficient coding scheme for neural networks. In: Eckmiller, R., Hartmann, G., Hauske, G. (Eds.), Parallel processing in neural systems and computers. North-Holland Elsevier, pp. 91–94.

Thorpe, S., Delorme, A., Rullen, R. V., 2001. Spike-based strategies for rapid processing. Neural Networks 14, 715–725.

Thorpe, S., Fize, D., Marlot, C., June 1996. Speed of processing in the human visual system. Nature 381, 520–522.

Thorpe, S., Gautrais, J., 1998. Rank order coding. Computational Neuroscience: Trends in Research. J. Brower (ed), 113–119.

Tovée, M., Rolls, E., Treves, A., Bellis, R., August 1993. Information encoding and the responses of single neurons in the primate temporal visual cortex. Journal of Neurophysiology 70 (2), 640–654.

Uzzell, V. J., Chichilnisky, E. J., 2004. Precision of spike trains in primate retinal ganglion cells. J. Neurophysiol. 92, 780–789.

van Rullen, R., Gautrais, J., Delorme, A., Thorpe, S., 1998. Face processing using one spike per neurone. BioSystems 48, 229–239.

Warland, D., Reinagel, P., Meister, M., 1997. Decoding visual information from a population of retinal ganglion cells. J. Neurophysiol 78, 2336–2350.

Winzenborg, I., 2007. Bayes'sche schaetztheorie und ihre anwendung auf neuronale daten zur reizrekonstruktion. Tech. rep., Carl von Ossietzky Universitaet von Oldenburg.

Winzenborg, I., Thiel, A., Harmand, P., Greschner, M., Kretzberg, J., March 2010. Stimulus- and response-triggered reconstruction of stimulus motion features based on spike rates and response latencies. Submitted.

Wässle, H., 2004. Parallel processing in the mammalian retina. Nature reviews. Neuroscience 5, 1–11.

Yarbus, A., 1967. Movements of the Eyes. Plenum, New York.

Zhang, K., Ginzburg, I., McNaughton, B., Sejnowski, T., 1998. Interpreting neuronal population activity by reconstruction: Unified framework with application to hippocampal place cells. J. Neurophysiol 79, 1017–1044.

Acknowledgments

After nearly three years of work at the International Graduate School for Neurosensory Science, Systems, and Applications (DFG Graduiertenkolleg 591, InterGK) as well as at the Institute for Chemistry and Biology of the Marine Environment (ICBM), I can say that it was a pleasure to collaborate and interact with colleagues (graduates and senior scientists) from diverse fields of research. It will be hard to mention everyone by name who contributed in one way or the other to the successful completion of the present work. While Jan Freund as my thesis advisor provided me with a lot of support for the writing of manuscripts and the work on the theoretical concepts, I also enjoyed the helpful discussions with Jutta Kretzberg, Josef Ammermüller, Andreas Thiel, León Juárez and José Manuel Ferrández. Of course I would not have been able to begin my research without the kind supply of experimental data by Martin Greschner. Certainly, the present thesis would have been completely different (i.e. worse) without the discussions and meetings with other graduate students directly or indirectly involved in the InterGK.

I also wish to thank all the members of the complex systems research group at the ICBM who were always at hand when I needed help. I am especially grateful to Jöran März who helped me a lot with typesetting this work in LATEX, to Klemens Buhmann who assisted me in the case of computer problems, and to Nico Grüner who helped me with translations from English to German. Last but not least I wish to express my deepest gratitude to all my friends and family who accompanied me along my way despite the distance. My parents William and Gladys, my sisters Gina and Lorena, my loving girlfriend Erika, and all my friends have provided help and comfort whenever necessary.

Curriculum Vitae

Persönliche Daten

Nachname:	Cerquera Soacha
Vorname:	Edwin Alexander
Geburtsdatum:	12.08.1978
Staatsangehörigkeit:	kolumbianisch
Geburtsort:	Bogota, Republik Kolumbien
Familienstand:	ledig

Schule & Studium

04/2007–07/2010	Promotionsprogramm "Neurosensory Science and Systems". Fakultät für Mathematik und Naturwissenschaften. Carl von Ossietzky Universität Oldenburg. Deutschland.
02/2004–02/2006	Magisterprogramm des Ingenieurwesens industrielle Automatisierung. Fakultät für Ingenieurwissenschaft und Architektur. Nationale Universität von Kolumbien. Manizales, Republik Kolumbien.
08/1995–08/2002	Ingenieurwesen für biomedizinische Technik. Fakultät für Ingenieurwissenschaft der Elektronik und der biomedizinischen Technik. Antonio Nariño Universität. Bogota, Republik Kolumbien.

Arbeitserfahrung

Seit 02/2006	Forschung und Lehre an der Antonio Nariño Universität in Bogota, Republik Kolumbien.
	Lehreaktivität an der Fakultät für Ingenieurwissenschaft der Elektronik und der biomedizinischen Technik. Die Fächer, die ich dort übernahm, lagen im Bereich der

biomedizinischen Signalverarbeitung. Außerdem analysierte ich elektrokardiographische Signale bei Hunden an der Forschungsgruppe für komplexe Systeme. Ich habe zurzeit ein Stipendium im Rahmen eines Kooperationsvertrages zwischen der Antonio Nariño Universität und dem DAAD, um meine Promotion an der Carl von Ossietzky Universität Oldenburg anzufertigen (Stipendienprogramm ALECOL).

10/2007–02/2008 und 10/2008–02/2009 Lehrtätigkeiten als Tutor in einem Programmierkurs (Matlab) an der Carl von Ossietzky Universitat Oldenburg.

08/2004–11/2005 Forschung und Lehre an der nationalen Universität von Kolumbien in Manizales, Republik Kolumbien.

Lehreaktivität an der Fakultät für Ingenieurwissenschaft und Architektur. Im Rahmen meines Magisterstudiums analysierte ich phonokardiograpische Signale an der Forschungsgruppe für Kontrolle und digitale Signalverarbeitung. Ich betreute auch Praktika von Studenten der Ingenieurwissenschaft, um meine Forschung zu unterstützen.

05/2005–12/2005 Forschung an der Universität von Caldas. Manizales, Republik Kolumbien.

Ich absolvierte mein Magisterstudium im Rahmen einer Kooperation mit dieser Universität, in der ich 20 Stunde pro Woche arbeitete. Meine Arbeit beruhte auf der Anwendung von Computertechniken, um Herzgeräusche zu identifizieren. Diese Forschung wurde im Rahmen des Projektes *Auskultation und elektrokardiographische Registrierung am Web, um ärztliche Fernuntersuchung zu unterstützen* durchgeführt.

Oldenburg, Deutschland, 7. Juli 2010

Erklärung

Hiermit erkläre ich, dass ich die vorliegende Dissertation selbstständig verfasst habe und nur die angegebenen Hilfsmittel verwendet habe. Teile der Dissertation wurden bereits veröffentlicht bzw. sind zur Veröffentlichung eingereicht, wie an den entsprechenden Stellen angegeben. Die Dissertation hat weder in Teilen noch in ihrer Gesamtheit einer anderen wissenschaftlichen Hochschule zur Begutachtung in einem Promotionsverfahren vorgelegen.

Oldenburg, den 7. Juli 2010.

_____

Edwin Alexander Cerquera Soacha